Natural Resources Canada | Ressources naturelles Canada

GEOLOGICAL SURVEY OF CANADA
OPEN FILE 8101

Overview of the 2013 and 2014 Baseline Magnetotelluric & Controlled Source Electromagnetic Studies of CO_2 Sequestration at the Aquistore site near Estevan, Saskatchewan

J. McLeod, J.A. Craven, I.J. Ferguson and B.J. Roberts

2016

Canada

GEOLOGICAL SURVEY OF CANADA
OPEN FILE 8101

Overview of the 2013 and 2014 Baseline Magnetotelluric & Controlled Source Electromagnetic Studies of CO_2 Sequestration at the Aquistore site near Estevan, Saskatchewan

J. McLeod[1], J.A. Craven[2], I.J. Ferguson[1] and B.J. Roberts[2]

[1]University of Manitoba, Winnipeg, Manitoba
[2] Geological Survey of Canada, Ottawa, Ontario

2015

doi:10.4095/ 299100

This publication is available for free download through GEOSCAN (http://geoscan.nrcan.gc.ca/).

Recommended citation
McLeod, J., Craven, J.A., Ferguson, I.J., and Roberts, B.J., 2015, Overview of the 2013 and 2014 baseline magnetotelluric & controlled source electromagnetic studies of CO_2 sequestration at the Aquistore site near Estevan, Saskatchewan, Open File 8101, 44p. doi:10.4095/ 299100

Publications in this series have not been edited; they are released as submitted by the author.

Figures & Tables

Introduction

The Aquistore project is a large-scale carbon dioxide (CO_2) capture and sequestration initiative, taking place to the southwest of Estevan, Saskatchewan. Emissions of CO_2 generated from SaskPower's nearby Boundary Dam Power Station are to be captured and injected, in liquid form, deep into stable sedimentary packages of the Williston Basin for long-term storage (Aquistore, 2013). The overall aim of the project is to reduce greenhouse gas emissions coming from a fixed source of CO_2 discharge, while demonstrating the effectiveness of using geological formations as a sequestration reservoir (Whittaker and Worth, 2011). Carbon capture and storage (CCS), in combination with renewable energy technologies, is potentially a strong means of mitigating anthropogenic climate change.

The Aquistore reservoir will be the Cambro-Ordovician aquifer system of the Deadwood and Winnipeg Formations of the Williston basin which forms part of the Western Canada Sedimentary Basin (Aquistore 2013). The primary target is at 3400 m depth, which is deep in comparison to other CO_2 site studies. The reservoir at Ketzin is at 635-650 m depth, at Hontomín it is at 1350-1460 m, and at Kevin Dome it is at 3000 m. The Aquistore target lies beneath a thick sequence of very conductive (<10 Ω.m) rocks of the Jurassic to Paleocene Zuni succession (Jones 1988, Gowan et al., 2009). The surface environment in the study area includes a number of possible sources of electromagnetic noise including infrastructure of the Boundary Dam Power Station and Prairie farming operations. The electromagnetic noise may create challenges for both controlled source and natural source measurements (Ferguson, 2012; Escalas et al., 2013).

The project discussed herein focuses on the application of surface controlled-source and natural source electromagnetic (EM) monitoring methods at the Aquistore site. These methods provide an economic complement or alternative to surface seismic methods for defining the properties of the host geological structures and for the monitoring of CO_2 injection. Borehole EM measurements will provide superior resolution of a target CO_2 plume than surface EM measurements (e.g., Vilamjó et al., 2013) but downhole electrodes have not been installed at Aquistore. Surface EM measurements have the advantages of allowing a much larger signal level and eliminating the need for subsurface borehole access to deploy monitoring sensors. To date, relatively few such measurements have been made in association with CO_2 storage projects. Examples of land sites at which surface EM methods have been modelled or applied include proposed CO_2 sequestration sites at Kevin Dome in the United States (Zhdanov et al., 2013), Ketzin in Germany (Streich et al., 2011) and Hontomín in Spain (Ogaya et al., 2013). Related studies have also been conducted at geothermal sites, e.g., the Paralana site in Australia (Peacock et al., 2013). In the future, feasibility modeling will be conducted to assess the sensitivity of surface EM measurements to the displacement of brine by CO_2, the dissolution of CO_2 within the brine in the reservoir, and leakage into the overlying strata.

A component of the surface controlled-source EM (CSEM) investigations at Aquistore includes a survey by British Petroleum (BP) and GroundMetrics, Inc. (GMI) using a novel borehole to surface electromagnetic (BSEM) survey configuration (Hibbs, 2013). This method injects an electric current using a surface array of electrodes oriented radially to the well. Measurement at the surface of the

distribution of electric current that return from reservoir depths via the injection well casing provides a means to detect signals from reservoir depths.

Surface EM investigations at Aquistore use the natural-source magnetotelluric (MT) method and CSEM investigations use a surface electric bipole source along with electric dipole and magnetic sensors. Baseline MT and CSEM data were collected in 2013 and a repeat baseline MT survey was completed in 2014. This report provides an update on the acquisition and processing of the 2013 and 2014 surface EM data from the site. McLeod et al., (2014) describe the acquisition and preliminary processing of the 2013 data. Introductory material on the Aquistore site and electromagnetic study is included in the present report for completeness.

Overview of the Aquistore Project

Prior to being released into the atmosphere, the waste gases created the Boundary Dam power station will be treated with an amine solvent to remove CO_2. The CO_2 is then dehydrated and compressed for transportation and storage, while the solvent undergoes a heating and cooling cycle that allows it to be reused (Gibbins and Chalmers, 2008). Captured carbon products will be transported to the injection well via pipeline. Of an anticipated 3,000 tons of CO_2 captured by SaskPower each day, 2,000 tons are destined for geological storage. The remaining CO_2 will be sold to Cenovus Energy for the purposes of enhanced oil recovery (Aquistore, 2013; SaskPower, 2013).

A number of factors make the Winnipeg and Deadwood formations in the Williston Basin ideal targets for CO_2 sequestration. This section of the sedimentary sequence consists of porous rock, capable of storing vast amounts of injected fluid. At depths greater than 3 km, these formations lie beneath the region's oil reservoirs, potash-bearing rocks, and exploited groundwater aquifers and have no economic value themselves (Aquistore, 2013). Impermeable layers seal the reservoir from potential leakage. The tectonically stable setting of the Williston Basin is also an important aspect for the long-term storage goals (Aquistore, 2013).

A crucial part of the project is monitoring of the subsurface response to the injected fluid. The continued injection of CO_2 will be dependent on the integrity of the sealing units and on the subsurface distribution of the fluid. A suite of monitoring techniques are being utilised at the Aquistore site to ensure that these requirements are being satisfied at multiple stages of the injection (Aquistore, 2013).

The intent of the NRCan Integrated CO_2 Measurement, Monitoring & Verification Study is to simultaneously test and calibrate monitoring tools (other than seismics) at the CO_2 injection site. 3D time-lapse seismic methods have been the predominant monitoring tool utilized in pilot CO_2 injection/storage projects. Other less intensive monitoring methods are desirable to either complement or substitute for seismic methods. Ultimately, the observations will be quantitatively integrated to estimate the subsurface distribution of CO_2 and ground deformation that may affect the integrity of the storage complex. From this comprehensive monitoring suite, a minimum set of tools can be tailored to achieve the required goals in future monitoring programs.

As a subset of Aquistore's monitoring program, this research will employ EM techniques to image the host geological structure at the site, define the ambient EM noise levels, examine the resolution and repeatability or natural-source and controlled-source EM methods, and, if feasible, provide time-lapse mapping of the CO_2 plume. MT and CSEM data collected at the Aquistore site will be used to produce repeat images of the electrical properties of the storage complex as the CO_2 is being injected. Electromagnetic monitoring of electrical conductivity at sub-surface injection and extraction sites can provide valuable constraints on changes in fluid content and fluid salinity. We seek to test if characteristic electrical resistivity signature in images derived from the MT and CSEM data will serve as a proxy for the concentration and spatial distribution of CO_2. At Aquistore, seismic surveys will predominate in the characterisation of the evolving reservoir (Aquistore, 2013). The extent to which EM methods could be a source of complementary information to the existing time-lapse seismic methods will also be assessed over the life of the NRCan study.

Geological Setting

Williston Basin

The Williston Basin is a large intracratonic sedimentary basin that extends from southern Saskatchewan and southwest Manitoba into Montana and South Dakota (Figure 1). The basin lies unconformably above a basement of Archean and Proterozoic-aged cratons (Fowler and Nisbet, 1984). In east-central Saskatchewan, the basin thickness is between 2.2 and 3 km (Whittaker and Worth, 2011). Ages of the constituent strata range from middle Cambrian to early Cenozoic. Continuous subsidence from the Cambrian to the Jurassic is suggested as the driving mechanism of the Williston Basin's development (Fowler and Nisbet, 1884). The subsidence following the Jurassic is noted to be more complex and influenced by tectonic forces to the west. Alternatively, Zhu and Hajnal (1993) propose nine distinct episodes of subsidence interpreted from seismic data.

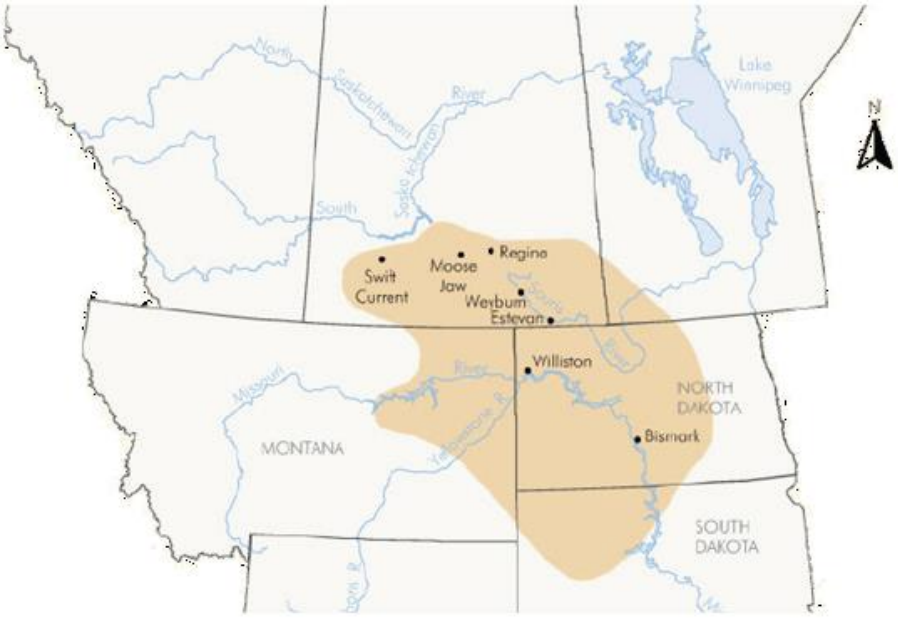

Figure 1 Aerial extent of the Williston Basin (Whittaker and Worth, 2011).

The Basin's sedimentary record is incomplete. Unconformities from periods of erosion and non-deposition correlate well with changes in sea level (Figure 2) (Fowler and Nisbet, 1984). The deepest rocks of the basin are the sandstones of the Deadwood Formation, which are separated from the Precambrian rocks below, and the Middle Ordovician Winnipeg formation above by erosional unconformities. The Winnipeg Formation consists of sandstone and shales, and is a part of the Tippecanoe sequence (Binda and Simpson, 1989). Carbonates, evaporites and shales characterize the overlying Kaskaskia sequence. The Triassic shales of the succeeding Lower Watrous Formation are unconformably overlain by the Jurassic evaporites of the Upper Watrous. This sequence lies beneath the Zuni sequence and surficial glacial deposits of the Pleistocene (Gowan et al., 2009). Collectively, the strata of the Williston Basin form alternating sequences of aquifers and aquitards (Figure 3).

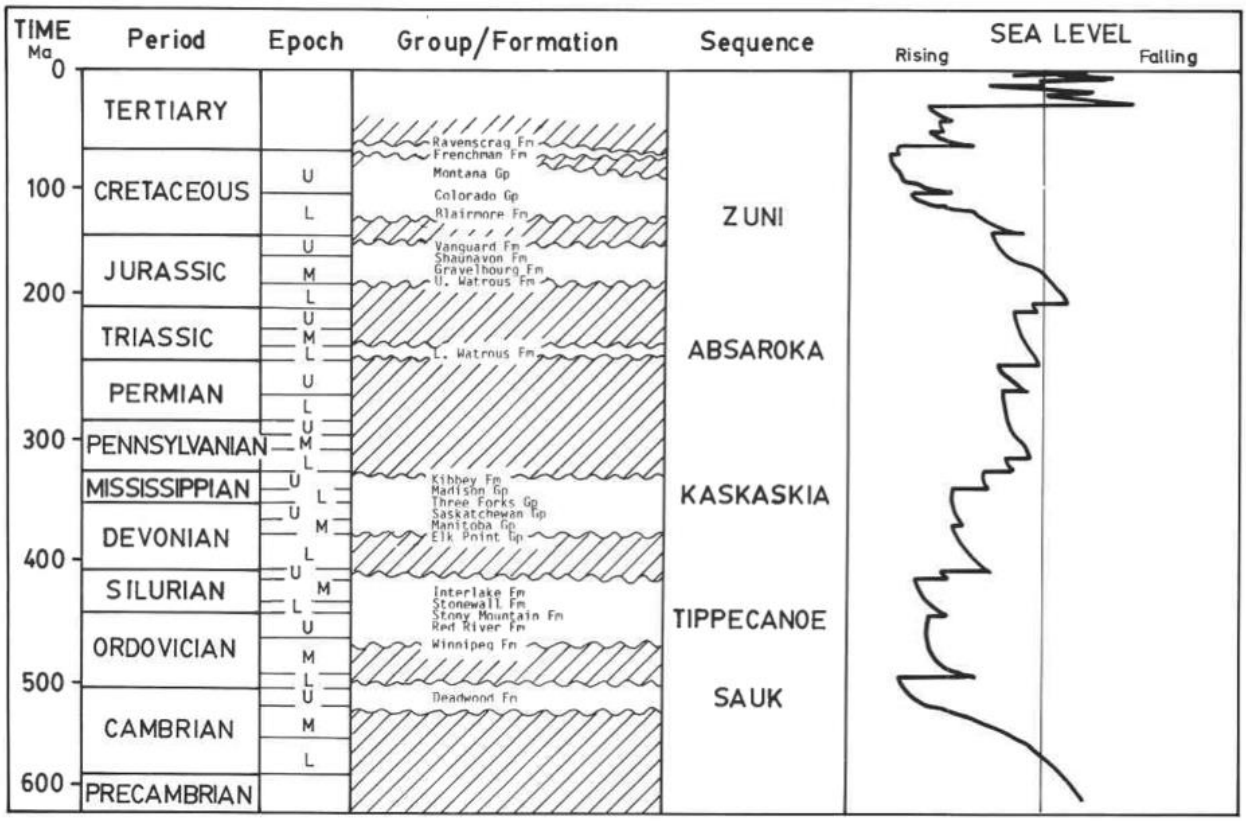

Figure 2 Regional stratigraphy of the Williston Basin in Saskatchewan (Fowler and Nisbet, 1984).

Deadwood Formation

The Cambro-Ordovician Deadwood formation lies unconformably above the Precambrian basement, and is the basal unit of the Williston Basin in the study area. Moving west, the unit thickens rapidly, and is underlain by the Earlie Formation and Basal Sandstone unit (Maclean, 1960; Dixon, 2008). In the eastern portion of the Williston Basin, the Deadwood Formation is predominantly a sandstone layer, whereas in Alberta, the formation consists mostly of shales. Sandstones of the northern Deadwood Formation are highly glauconitic. The sandstones become more quartzose and

generally coarser grained to the south (Maclean, 1960). Interbeds of silty and shaly rocks in the Deadwood add heterogeneity to the unit (Whittaker and Worth, 2011). The beds of the formation show an upward coarsening character (Dixon, 2008).

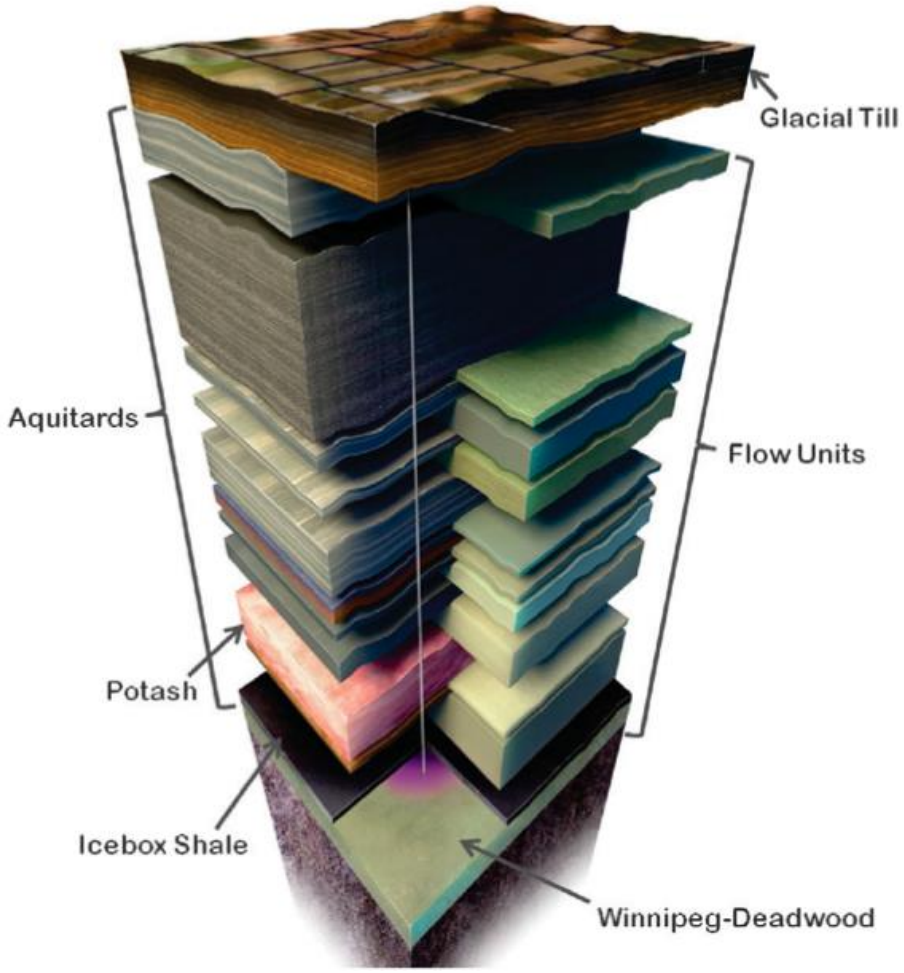

Figure 3 Hydrostratigraphy of the Williston Basin at the Aquistore site (Whittaker and Worth, 2011).

Winnipeg Formation

The Winnipeg Formation is predominantly a sandstone aquifer, deposited in the Middle to Late Ordovician following early subsidence in the Williston Basin (Smith and Bend, 2004). It lies unconformably overtop of the Cambrian to Lower Ordovician Deadwood Formation, and near the edges of the Williston Basin, the Precambrian basement (Figure 4). In North Dakota, the Formation reaches a maximum thickness of over 100 m (Binda and Simpson, 1989).

Subdivisions of the Winnipeg Formation include the Black Island, Icebox and Roughlock members (Smith and Bend, 2004; Ferguson et al., 2007). The Black Island package is the lowest member in the formation and consists of well to poorly-sorted quartzose sandstone. The Black Island sandstones are differentiated from the Deadwood Formation by a higher textural and mineralogical maturity, an absence of glauconite, and lower gamma-ray log radioactivity counts (Binda and Simpson,

1989). Lying conformably above of the Black Island sandstones are the shales of the Icebox member. These shales have been interpreted as an extensive flooding surface (Smith and Bend, 2004). The Roughlock member is the uppermost subunit of the Winnipeg Formation. Where present, the Roughlock provides a smooth transition from the Icebox member to the overlying carbonates of the Upper Ordovician Red River Formation. However, the Icebox member is not present in most of Saskatchewan, and in these areas, the contact between the Red River and Winnipeg formations is unconformable (Smith and Bend, 2004). At the Aquistore site, the Icebox member will serve as the primary seal for the injected fluid (Whittaker and Worth, 2011).

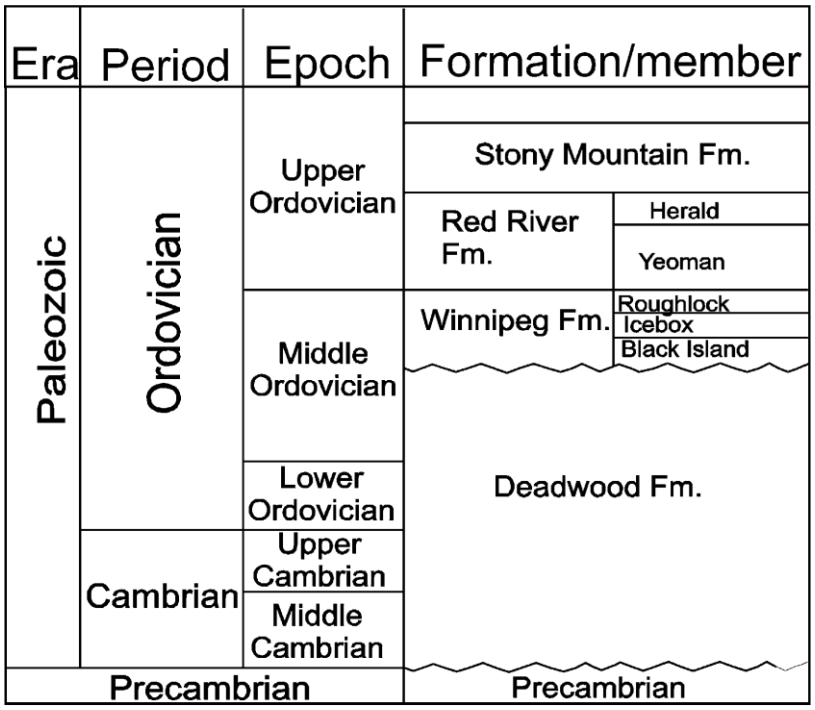

Figure 4 Stratigraphic section of the lower Williston Basin (Smith and Bend, 2004).

Background Electromagnetic Theory

Previous Synthetic and Field EM Studies of CO_2 Sequestration

Electromagnetic geophysical techniques detect variation in the electrical resistivity of the subsurface materials and fluids. A number of petrophysical models numerically quantify the relationship between pore fluid resistivity and the resistivity that can be inferred from an EM study. These models are based on various factors including pore geometries, clay content and interconnectivity and salinity of the pore fluid. Due to density contrasts, it is expected that CO_2 and brine will largely separate in the reservoir (Huang et al., 2014). In a lab experiment, Fleury and Deschamps (2008) found that as CO_2 was introduced to a saline solution, the resistivity changed according to the following simple function of temperature (T, ^{o}C) and molar fraction of CO_2 (x_{CO_2}):

$$\rho(x_{CO_2}, T) = \left[\rho(x_{CO_2}, T_o)(1 - 6.0x_{CO_2})\left(\frac{T + 19.5}{T - 19.5}\right)\right]^{-1} \quad (1)$$

Incorporation of equation (5) into a simple petrophysical model from Archie (1942) results in resistivity dependant on molar fraction CO_2 and a range of reservoir porosities (Figure 5). More recent laboratory studies of the CO_2 system include those of Börner et al. (2013, 2015) and Bosch et al. (2016). The implication is that methods to detect a temporal change in electrical resistivity at depth will image a temporal change in the mole fraction of CO_2 within the aquifer, under the condition that all else remaining constant. As the injection proceeds EM methods should, in theory, be able to detect the spatial progression of the plume away from the injection well; and may be able to detect leakage through overlying aquitards if the experiment is designed to explore at the proper range of depths.

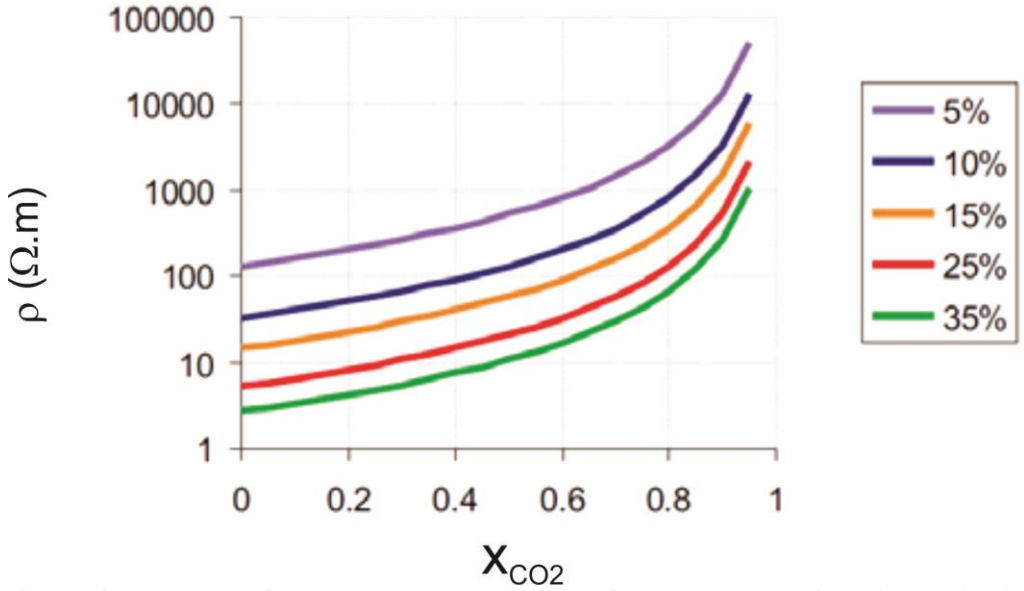

Figure 5 Bulk electrical resistivity with increasing CO_2 saturation and varying porosity from 5% to 35% (After Jones, 2013).

MT and controlled-source methods have previously been used to characterize CO_2 storage complexes in Hotomín, Spain and Ketzin, Germany (e.g. Streich, 2016). At the Hotomín site, pre-injection studies indicate that the contrast in electrical resistivity of the reservoir rock and the primary seal is sufficient to identify any changes in the rock properties following an injection (Ogaya, et al., 2013). It is anticipated that the CO_2 will introduce a detectable high resistivity signature to the host aquifer (Vilamajo et al., 2013). Numerical modelling of the feasibility of detecting CO_2 plumes near Ketzin using CSEM methods offer mixed results. Streich et al. (2010) conclude that CO_2 may be clearly identified using EM methods, but that not all source-receiver configurations provide the resolution needed to observe growth of the plume over time. Vertical electric field sensors placed in boreholes would be ideal for CO_2 detection.

The MT Method

The MT method relies on naturally occurring geomagnetic variations to induce electric currents in the Earth's subsurface and has the advantage of not requiring the costly and time consuming

deployment of an artificial EM source. Orthogonal components of the secondary magnetic and electric fields arising naturally from the currents are recorded as time series at the surface. The underlying geoelectric structure may then be inferred from the relationships between these field components (see for example Vozoff, 1991; Simpson and Bahr, 2005).

Horizontal electric and magnetic field components are related by the impedance tensor, ***Z***:

$$\begin{pmatrix} E_x \\ E_y \end{pmatrix} = \begin{pmatrix} Z_{xx} & Z_{xy} \\ Z_{yx} & Z_{yy} \end{pmatrix} \begin{pmatrix} H_x \\ H_y \end{pmatrix} \quad (2)$$

The significance of the impedance tensor is its description of the dimensionality and strike of the subsurface resistivity structure. The impedance elements are determined using auto- and crosspowers of the frequency-domain field components. The determination of the impedance often will include remote-referenced data (Gamble et al., 1979) to minimize local noise on magnetic field components. It is convenient to express the impedance magnitude in terms of the apparent resistivity as:

$$\rho_{a,ij}(\omega) = \frac{1}{\mu_0 \omega} \left| Z_{ij}(\omega) \right|^2 \quad (3)$$

The different types of geoelectric structure that might be encountered are: 1D, where resistivity varies only with depth; 2D, where resistivity varies with depth and one horizontal direction; and 3D, where resistivity varies in all spatial directions. The 1D and 2D (for a coordinate system aligned with geoelectric strike) scenarios will produce characteristic impedance tensors (Vozoff, 1991; Simpson and Bahr, 2005). The EM signals in 2D structure are commonly separated into TE (current flow is parallel to the strike) and TM (current flow is perpendicular to strike) modes. Knowing the strike and dimensionality of the subsurface structure will permit informed choices of inversion methods, and superior models of the subsurface resistivity structure.

Although relatively inexpensive and comparatively easy to deploy, an MT survey is unlikely to be sensitive to a thin resistor (i.e. the CO_2) at a depth of 3400 m due to the inherent lack of sensitivity of inductive EM techniques to such features. Inductive techniques rely primarily on the generation of electric currents within conductive material to provide a detectable signal that can be used to infer subsurface properties. Nonetheless, MT can provide an estimate of the background (i.e. regional) electrical structure associated with the Williston Basin and the underlying basement and constrain uncertainties in the analysis of other datasets sensitive to similar rock properties. To provide direct detection of thin resistors at depth resulting from CO_2 injection it is advisable to use CSEM methods as they inject a current vertically and the resulting spatial current distributions and electric fields will be noticeably affected upon encountering the resistive layer.

Controlled-Source Electromagnetism

Controlled source EM geophysical exploration has undergone a resurgence primarily within the marine oil & gas industry (e.g., Streich, 2015). One of the proven advantages of the marine CSEM technique is its ability to detect thin resistive layers at considerable depths (e.g. Johansen et al., 2005). It has been also been shown that the imaged resistivity of the thin layer correlates reasonably well with the oil saturation within the layer. In a typical marine CSEM project a dipole transmitter is lowered off a ship to a point close to the seabed and receivers are deployed on the seafloor in a profile behind the

ship. In such a configuration it is possible to explore for thin resistors (using low frequency sources) at depths of over 4 km depending on local conditions. To a large extent, the key anomalous response to detect the thin layer is exhibited in the component of the electric field parallel and in-line with the transmitter bipole. Gasperikova and Hoversten (2006) have demonstrated that terrestrial CSEM techniques can be sensitive to CO_2 content of layers > 1 km in depth and to movement of the fluids within the layer of the order 500 m. The primary purpose of this open file is to document the 2013 and 2014 field experiments and preliminary results.

NRCan EM studies at Aquistore

The specific objectives of the NRCan EM studies at Aquistore are to image the host geological structure at the site, define the ambient EM noise levels, to examine the resolution and repeatability or natural-source and controlled-source EM methods, and, if feasible, to provide time-lapse mapping of the CO_2 plume. A series of baseline EM measurements has been made prior to the start of CO_2 injection, including field campaigns in 2013 and 2014, to achieve the first three specific objectives.

The pattern of MT and CSEM recording sites was designed in order to be able to discern the response of an expected predominantly radially-distributed CO_2 plume (Whittaker and Worth, 2011). Individual site locations were chosen to as to provide optimal MT and CSEM responses. The surveys were based on a profile of sites over the injection well with the intersite distance increasing with distance from the well (Figures 6 and 7). The profile azimuth was chosen in order to align with the regional fluid flow in this portion of the Williston Basin (Bachu and Hitchon, 1996) as it is expected that this flow may have a small influence on the radial outward progression of the injected fluids. The bipole transmitter centred ~3.5 km northeast of the well was aligned with this profile. Additional EM sites were deployed to the northwest and southeast of the central part of the line to provide 2-D MT coverage. The MT and CSEM sites recorded in 2013 (McLeod et al., 2013) are shown in Figure 6 and the MT sites recorded in 2014 are shown in Figure 7.

Data Acquisition and Processing

Overview

Baseline EM data were collected during two field surveys separated by approximately fourteen months. The first dataset, collected from August 21st to 28th, 2013, contains both CSEM as well as MT data. The second dataset, collected from November 6th to 12th, 2014, is exclusively MT data. The MT surveys included acquisition of broad-band MT and audio-frequency MT (AMT) responses.

In general, spatial variations of the electric field are more rapid than variations of the magnetic field so in MT surveys with closely spaced sites such as the Aquistore survey it is possible to maximize the survey efficiency by recording the electric field at each site but the magnetic field at only selected sites. This procedure was followed in the Aquistore survey. The MT and AMT responses were calculated for each site using the local electric field data and either locally recorded AMT and MT data or AMT or

MT recordings imported from a nearby site. Table 1 documents the sites at which the MT and AMT sensors were installed.

The MT surveys employed a remote-reference site to allow noise reduction using the remote-reference impedance-determination method. A remote site (aqi02) was located a significant distance to the southwest, in a region free of man-made infrastructure and possible noise sources (Figure 6) and was used to collect MT data during the 2013 and 2014 surveys. A superior remote reference site was established to the northeast of Estevan during the 2014 survey (Figure 7). For AMT processing, the remote site was chosen from the sites available within the main survey area, as AMT coils were not installed at either of the MT remote sites. In general, night time recordings are preferable for calculation of the MT response due to the enhanced natural signal. Calculation of the daytime MT response is possible, but one must be careful to exclude time periods when noise sources or the CSEM transmitter are active.

Difficulties in processing the MT data at sites aqi01 and aqi07 in the 2013 survey were attributed to high noise levels at these sites and prompted the establishment of new sites at nearby locations (sites aqi05 and aqi13 respectively). The noise source at aqi01 could be related to distortion in the local current systems due to the nearby steel-cased injection and monitoring wells. The noise source at aqi07 may be related to solar powered electric fences <100 m from the site. Because aqi13 was also a noisy site, a further site, aqi14, was established for the 2014 survey (Figure 7).

The MT and AMT surveys were done using Phoenix MT equipment. The electric fields were recorded using porous pot electrodes and 25 m to 50 m long electric dipoles. Three different types of induction coils were used as magnetic field sensors for data acquisition: AMTC-30 coils for AMT recordings, and two different generations of MTC coils for MT recordings. The AMT coils measure signals from 10,000 to 0.1 Hz whereas the MT coils are sensitive to signals in the 400 to 0.00002 Hz range. During the 2013 survey it was found that it was not possible to use different generations of the MTC coils in a recording as this procedure results in incorrect calibration of the recorded data.

The MT instruments were deployed progressively across the survey area during the 2013 and 2014 field campaigns. During 2013 survey in particular, a number of configuration and deployment issues, such as the calibration issue noted above, resulted in the limited availability of appropriate magnetic field data for use in importation to the primary site and/or for use as the remote reference.

The surface transmitter for the 2013 CSEM study performed at the Aquistore site was a horizontal electric bipole (grounding points shown in Figure 6 August, 2013 survey layout.). It used a moment of 1188.6 m × 24.75 A. The waveform of the bipole was an alternating square-wave energized at range of frequencies. In the frequency domain the harmonics of the square waves can also be utilized to determine responses. The focus of the CSEM studies is the electric field responses so E-field sensors at each MT/CSEM site were used to record perpendicular horizontal components of the electric field. However, only the in-line components were recorded at the long offset CSEM sites. Where available, the complementary magnetic field measurements of the CSEM signal will provide additional constraints on the level of anisotropy and degree of heterogeneity in the survey area. In addition, the MT measurements collected simultaneous to the CSEM survey will serve to mitigate the influence of natural telluric noise in the CSEM data. This background noise may hamper the detection of weak CSEM signals from the deep reservoir. Site aqi02 was operated by GroundMetrics Inc. independently

after completion of the NRCan work in order to develop algorithms to predict and remove telluric noise during CSEM surveys.

Throughout the 2013 MT and CSEM surveys a variety of sampling rates and sounding configurations were utilized to facilitate either or both MT and CSEM calculations at the sites and to establish optimal field procedures for future surveys. The 2014 MT survey used a more consistent set of sampling procedures and yielded a more consistent and complete set of MT data than the 2013 survey.

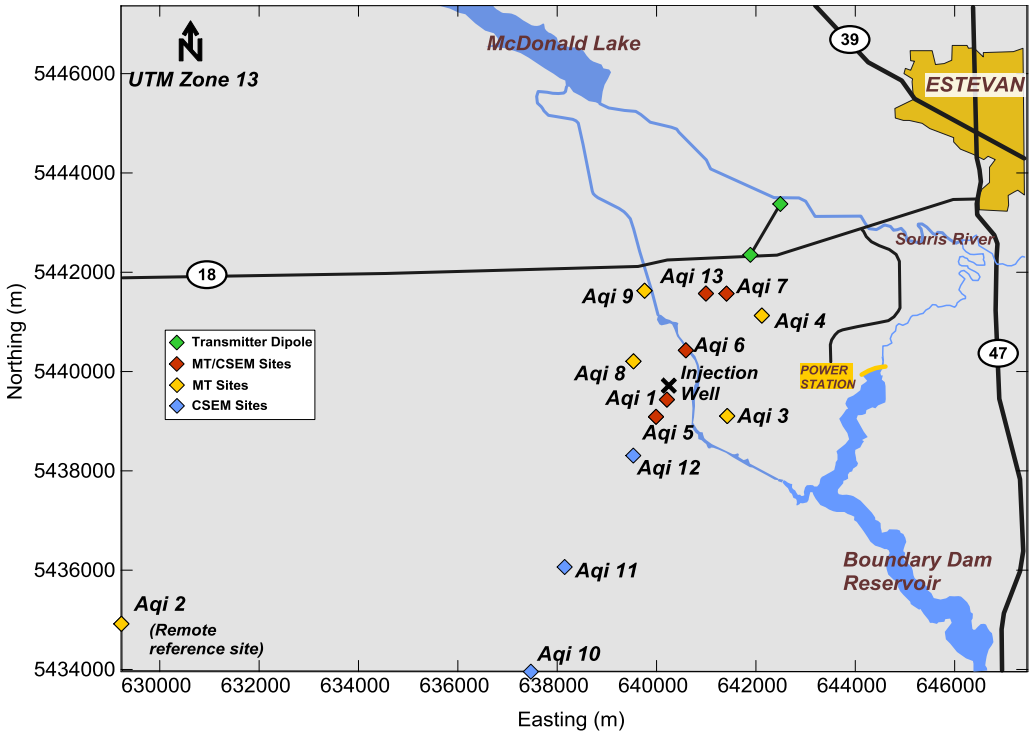

Figure 6 August, 2013 survey layout.

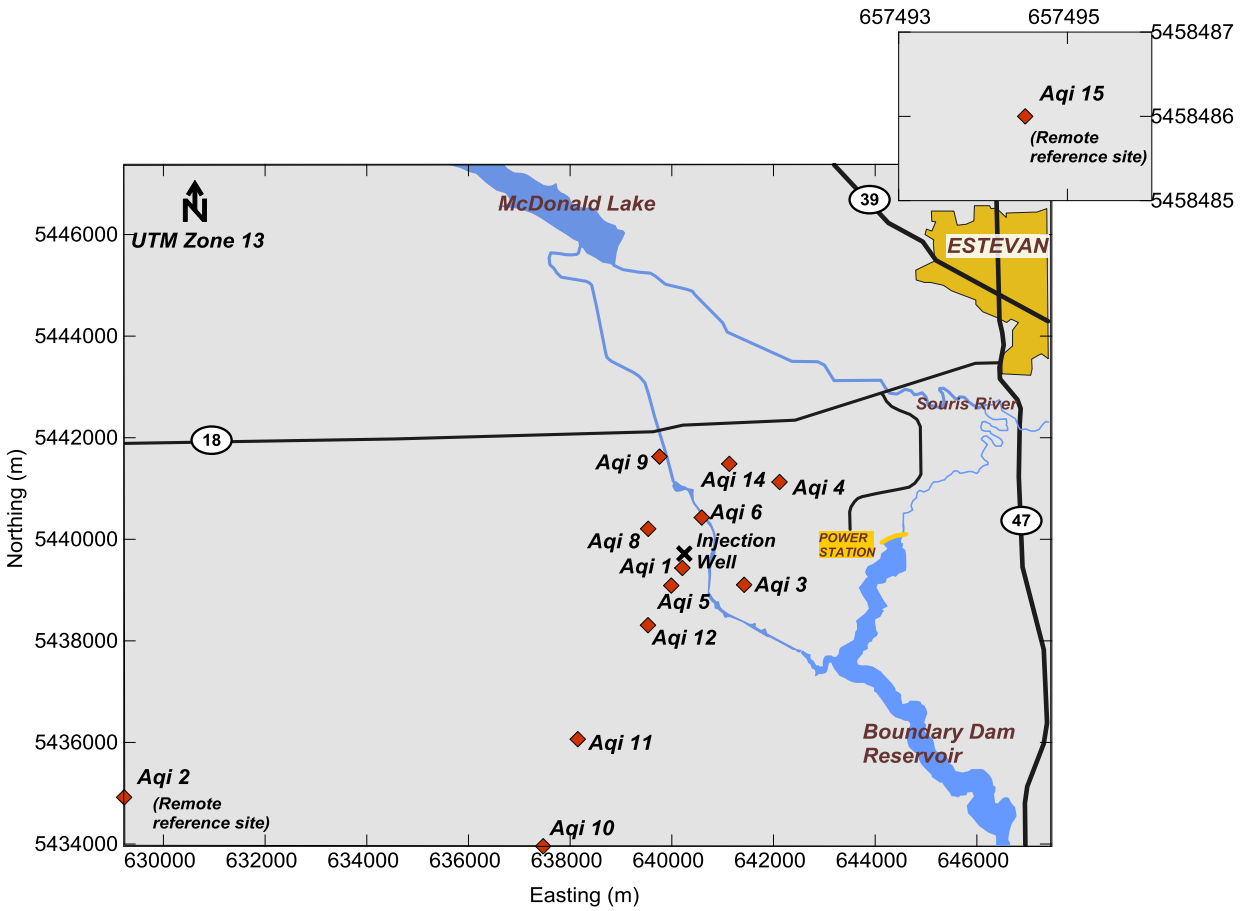

Figure 7 November, 2014 survey layout

The MT data processing was performed using a Phoenix Geophysics SSMT2000 software package. To date, MT and AMT processing has been performed, but the controlled-source data from August, 2013 has not been processed. Imported magnetic field data are chosen based on proximity to the site in question. The Fourier transforms were computed at 4 frequencies per octave. For robust processing, the time series were divided into 20 equal length segments from which crosspowers were calculated at the selected frequencies. Crosspowers were rejected if the coherency between the local and remote data was below a threshold of 0.35, or if the coherency between the telluric and magnetic data was below 0.25. The data were stacked with weights based on their error bars.

2013 Dataset

Table 2 provides a summary of processing of the 2013 MT data set. As noted above several issues affected the availability of magnetic field recordings in the processing. The mismatched coil pairs deployed at sites aqi03 and aqi09 caused problems on the magnetic channels that persisted through the processing (highlighted in Table 2). MT coils were in use at the remote sites on every day of data collection. So although the availability of local magnetic field data for MT processing was greatly restricted, the remote magnetic field data was able to be substituted for local magnetic recordings and local MT processing procedures were adopted.

	MT			AMT	
	2013	2014		2013	2014
aqi01	YES	YES	**aqi01**	NO	NO
aqi02	YES	YES	**aqi02**	NO	NO
aqi03	YES	NO	**aqi03**	NO	NO
aqi04	NO	NO	**aqi04**	YES	YES
aqi05	NO	NO	**aqi05**	YES	YES
aqi06	NO	NO	**aqi06**	NO	NO
aqi07	NO	N/A	**aqi07**	NO	N/A
aqi08	NO	NO	**aqi08**	YES	YES
aqi09	YES	YES	**aqi09**	NO	NO
aqi10	CSEM	YES	**aqi10**	CSEM	NO
aqi11	CSEM	NO	**aqi11**	CSEM	YES
aqi12	CSEM	NO	**aqi12**	CSEM	YES
aqi13	NO	N/A	**aqi13**	NO	N/A
aqi14	N/A	NO	**aqi14**	N/A	NO
aqi15	N/A	YES	**aqi15**	N/A	NO

Table 1 Deployment of MT and AMT sensors

For the aqi01 data from August 23rd 2013, the MT processing resulted in XY and YX apparent resistivity curves that are downshifted by approximately one decade (resembling a static shift). This gain problem was observed after importing this specific day of magnetic recordings to other sites for processing. All of the MT processing from this day is therefore affected, and these data did not contribute to the final edited MT data.

Controlled source data, collected on August 24th, 25th, 27th, and 28th 2013 were recorded either for short durations, or using only the E_X channel. For these reasons, these data was not processed with the MT/AMT data. The presence of both the bipole and GMI transmitters is visible in the MT/AMT data, but these signals were easily edited out as they operated at fixed frequencies. The aqi13 site, which was installed because the nearby aqi07 site was deemed too noisy, failed to process entirely. Likewise, the MT processing for sites aqi05 and aqi08 on August 26th also failed.

Table 2 Summary of processing on 2013 dataset.

		21-Aug	22-Aug	23-Aug	24-Aug	25-Aug	26-Aug	27-Aug	28-Aug
aqi01	MT			/aqi02					
	AMT		aqi05/aqi04	aqi05					
aqi03	MT		aqi01	aqi01/aqi02			aqi02		
	AMT			aqi05			aqi05/aqi08		
aqi04	MT		aqi01				aqi02		
	AMT		/aqi05				/aqi08		
aqi05	MT		aqi01	aqi01/aqi02	aqi02	aqi02			
	AMT		/aqi04		/aqi08	/aqi08	/aqi04		
aqi06	MT		aqi01	aqi01/aqi02	aqi02				
	AMT		aqi05/aqi04	aqi05	aqi08/aqi05				
aqi07	MT			aqi01/aqi02	aqi02	aqi02			
	AMT			aqi05	aqi08/aqi05	aqi08/aqi05			
aqi08	MT				aqi02	aqi02			
	AMT				/aqi05	/aqi05	/aqi04		
aqi09	MT				aqi02	aqi02			
	AMT				aqi08/aqi05	aqi08/aqi05			
aqi10	MT								
	AMT								
aqi11	MT								
	AMT								
aqi12	MT								
	AMT								
aqi13	MT								
	AMT								
GMI Tx		NO	NO	NO	YES	YES	YES	NO	NO
Bipole Tx		NO	NO	NO	NO	YES	NO	YES	YES

import	Local
loc/rem	Remote
	Failed to process
	CSEM only

2014 Dataset

There are fewer issues in the 2014 dataset, leading to a more straightforward processing sequence (Table 3). Almost all data were remote referenced. The second remote site, aqi15, was added after a 0.2 Hz signal was observed on the magnetic channels of aqi02 on November 6th. However, this signal was not observed on subsequent days. Unlike the 2013 dataset, full MT sites were installed at the remote locations, permitting processing of aqi02 and aqi15 data. Full processing was also done at sites aqi10, aqi11, and aqi12, which were previously used only for CSEM data acquisition. A problem with one of the MT recording units (MTU 1493) resulted in failed data collection on the electric field channels on three separate occasions. This issue is marked in Table 3 as 'failed to process'.

Table 3 Summary of processing on 2014 dataset.

		6-Nov	7-Nov	8-Nov	9-Nov	10-Nov	11-Nov	12-Nov
aqi01	MT		/aqi02	/aqi02			aqi10/aqi15	aqi10/aqi15
	AMT		aqi05/aqi04	aqi05/aqi04			aqi12/aqi11	aqi12/aqi11
aqi02	MT		/aqi01	/aqi01				
	AMT		aqi05/aqi04					
aqi03	MT		aqi01/aqi02					
	AMT		aqi05/aqi04					
aqi04	MT		aqi01/aqi02	aqi01/aqi02				
	AMT		/aqi05	/aqi05				
aqi05	MT		aqi01/aqi02	aqi01/aqi02	aqi09/aqi15			
	AMT		/aqi04	/aqi04	/aqi08			
aqi06	MT				aqi09/aqi15	aqi10/aqi15		
	AMT				aqi05/aqi08	aqi08/aqi12		
aqi08	MT				aqi09/aqi15	aqi10/aqi15		
	AMT				/aqi05	/aqi12		
aqi09	MT				/aqi15	aqi10/aqi15		
	AMT				aqi08/aqi05	aqi08/aqi12		
aqi10	MT					/aqi15	/aqi15	/aqi15
	AMT					aqi12/aqi08	aqi11/aqi12	aqi12/aqi11
aqi11	MT						aqi10/aqi15	aqi10/aqi15
	AMT						/aqi12	/aqi12
aqi12	MT					aqi10/aqi15	aqi10/aqi15	aqi10/aqi15
	AMT					/aqi08	/aqi11	/aqi11
aqi14	MT			aqi01/aqi02	aqi09/aqi15			
	AMT			aqi05/aqi04	aqi08/aqi05			
aqi15	MT					/aqi10	/aqi10	/aqi10
	AMT							

import	Local
loc/rem	Remote
	Failed to process

2013 Response Calculation

A further editing phase was required for all of the processed 2013 data. The editing consists of masking certain crosspower results for individual frequencies of the calculated response so that spurious or high-variance data are eliminated. An example of unedited data from aqi05 and August 25, 2013 is shown in Figure 8 Unedited processed MT response from aqi05, August 25, 2013.. The response from 0.1 s to 10 s is clearly affected strongly by noise. However, once combined with other processed data files of the same site, there were sufficient unaffected crosspowers to produce much higher quality responses (Figure 9). For the 2013 data set it was possible to define a smooth response over a broad frequency range at most sites. Noise is present in all the 2013 data, most notably from 0.125 to 6.667 s. In this period range, a decrease in signal coherence is observed at all sites, centered on a period of ~3 s (Figure 10). This broadband noise exists everywhere in the survey area, and affects the coherences for both locally and remotely processed data. The exception is coherence between the local H_Y and remote H_Y channels, which is usually significantly stronger in this period range.

The source of the noise can be examined using impedances calculated using either the local electric field or the local magnetic field as the remote reference. The magnitude of the former estimate (and the corresponding apparent resistivity) will be biased upwards relative to a true remote-reference response by noise on the electric field components and the magnitude of the latter estimate will be biased downwards by noise on the magnetic field components. In general, the data marked with a local E reference in the MT editor are biased upwards, especially the YX curves. The magnetically referenced data, and the XY curves in particular, are biased downwards, to a lesser extent than the local E referenced data. These observations indicate noise is present on all four horizontal electric and magnetic field channels, but that it is stronger on the electric field. It is notable that the magnetic noise was barely significant at the remote sites, but the E-field noise was present even in these distant areas.

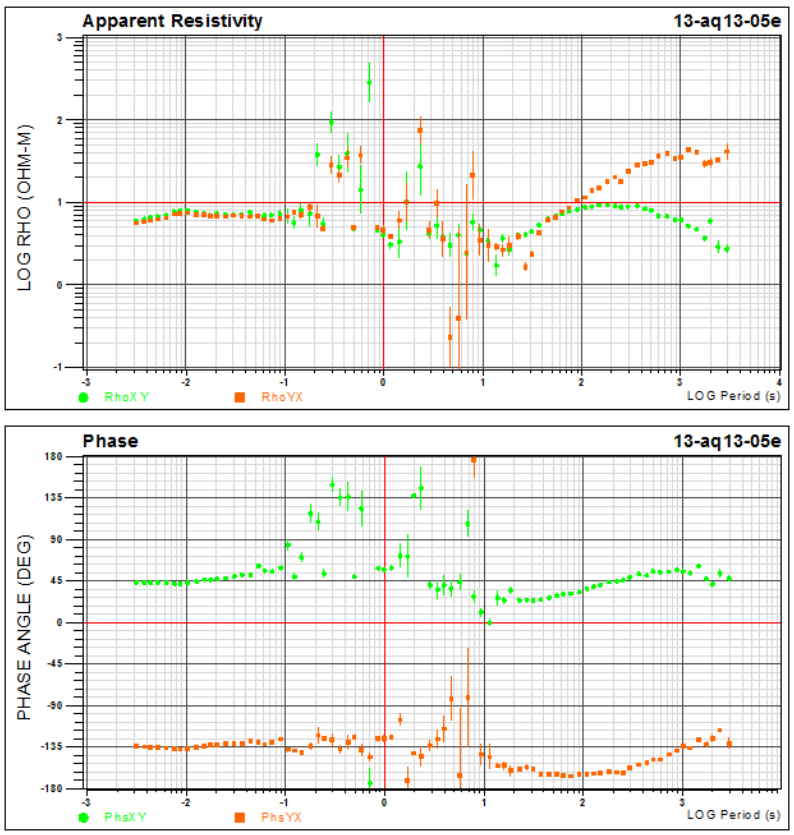

Figure 8 Unedited processed MT response from aqi05, August 25, 2013. Combined edited data from aqi05, 2013 survey. Top panel: apparent resistivity; bottom panel: phase.

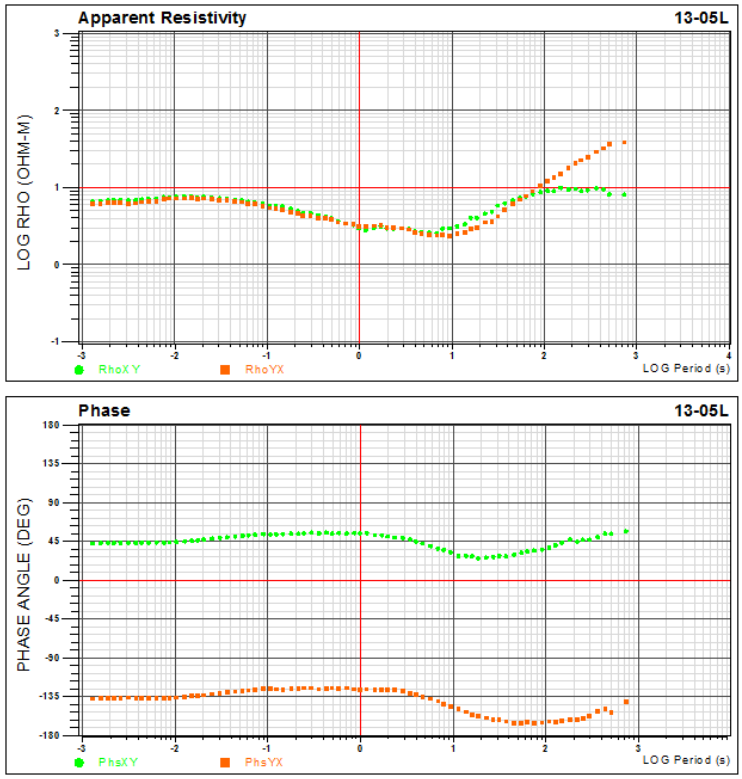

Figure 9 Combined edited data from aqi05, 2013 survey. Top panel: apparent resistivity; bottom panel: phase.

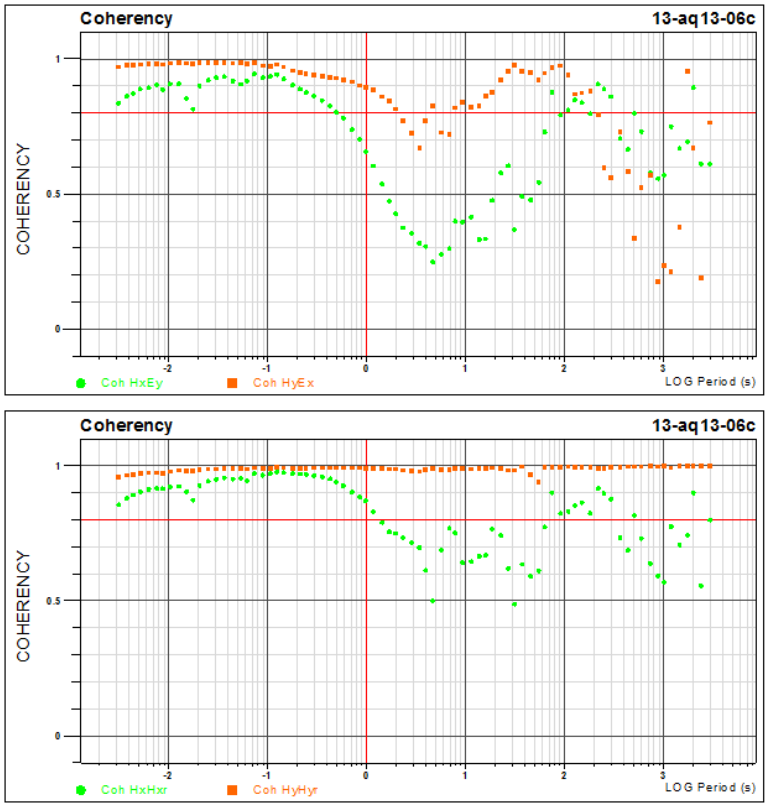

Figure 10 Coherence responses, aqi06, August 23, 2013. Top panel: coherences between local magnetic and telluric channels. Bottom panel: coherences between local and remote magnetic channels.

2014 Response Calculation

There is a significant amount of broadband noise present in the responses for the 2014 dataset. This noise is particularly evident in the 0 to 30 Hz and 85 to 140 Hz frequency ranges. The low frequency (long period) MT responses resemble those for the 2013 survey. However, irregular behaviour of the sounding curves is present at all periods shorter than 10 s. In this period range, the estimated impedances are higher than those indicated by the 2013 calculations. Coherences between the electric and magnetic fields decrease significantly in this noise band; the H_yE_x coherence is nearly zero from at all periods shorter than 1 s. However, the coherence between local and aqi02 remote H fields is strong, suggesting the presence of correlated noise across the survey area. Examination of the four impedance components shows that at some sites in the noise band the XX and YY impedance curves are shifted upwards by more than one order of magnitude and overlap the off-diagonal curves. This observation indicates that noise is polarized at an azimuth between the north-south east-west data acquisition coordinate system.

The editing process applied in 2013 was used again for the 2014 data. However, at most sites it was impossible to recover smooth impedances within the period band of the noise. The deletion of

calculated responses with spurious magnitudes or high-variance necessitated significant removal of broad bands of data during the editing stage.

General form of the MT responses

At periods less than 3 s, the edited MT responses show only slight variations from site to site, thus the shallow resistivity structure within the survey area can generally be characterized as one-dimensional. At short periods, the apparent resistivity values are ~6-10 Ω m. The MT response becomes more conductive beginning at a period of ~0.05 s, and continues on this trend to ~4 s. At this point the phases decrease indicating that the response is sensing an increase in resistivity associated with the Precambrian basement. At ~10 s, the XY and YX curves begin to diverge significantly, signaling multidimensional resistivity structure and a strong decrease in the contribution of the Phanerozoic rock to the response. From this point, the YX resistivity continues to become resistive up to the longest periods that were processed, whereas the XY resistivity levels off to 10 Ω m at 100 s.

The responses of the Williston Basin rocks are consistent with those determined in previous studies (Jones, 1988; Gowan et al., 2009). The divergence in the MT impedance components indicates a north-south trending conductive structure within the Precambrian rocks and this feature can be confidently interpreted as the North American Central Plains conductor (e.g., Jones and Craven, 1988; Jones, 1993; Jones et al., 2005).

Misfit Calculations

Long-term time-lapse monitoring of the injected CO_2 plume at Aquistore requires a consistent baseline of measurements from which deviations of the response due to evolution of the storage complex may be isolated. For the MT method, the ability to make accurately repeated measurements over time will depend on the extent to which a survey can be rerun in the field, and on the consistency of the determined responses in the presence of the local noise affecting the measurements. The repeatability of the MT method at the Aquistore site is defined here by computing a normalized root mean square (RMS) misfit between datasets collected in August of 2013 and November of 2014. Because of the extensive noise present in the 2014 data set, this analysis is primarily intended to define a methodology that can be applied in subsequent surveys. However, it also provides an initial indication of response repeatability for the parts of the MT responses that were not affected by the 2014 noise.

Comparison of the 2013 and 2014 datasets is done on a site-by-site and frequency-by-frequency basis, and requires that data from both surveys have followed a reasonably consistent processing and referencing scheme. Because the misfit measures used are based on individual frequency responses, there needs to be data from both 2013 and 2014 at a large number of common frequencies for the optimal calculation of the misfit. Unfortunately, due to extensive editing and limited availability of long-period responses, there is a limited amount of data available for the misfit calculations at some sites.

The normalized RMS misfit between datasets is given by:

$$E = \sqrt{\frac{1}{2n}\sum_{f=1}^{N}\sum_{i=1}^{2}\sum_{j=1}^{2}\frac{\left|Z(\omega_f)_{ij}^{2013} - Z(\omega_f)_{ij}^{2014}\right|^2}{\left|(Z(\omega_f)_{ij}^{2013})(Z(\omega_f)_{ij}^{2014})\right|}} \quad (4)$$

where $Z(\omega_f)_{ij}$ is the MT impedance data, N is the number of frequencies, and n is the total number of terms in the summation (Nx2x2), multiplied by 2 to account for two degrees of freedom from the real and imaginary parts of the impedance. This type of normalization, defined as **N1**, is based on a product of the impedance terms. An initial calculation used a product of data variances as a normalization term, but very small or poorly estimated variances values resulted in very large misfits. Two other normalization types that use only the off-diagonal tensor elements were tested: (i) assuming the errors are coming dominantly from the electric field, the Z_{xy} term was used for both the Z_{xx} and Z_{xy} terms and Z_{yx} for Z_{yx} and Z_{yy} (defined as **N2**), and (ii) for the case where the noise is assumed to be coming dominantly from the magnetic field Z_{xy} term was used for both the Z_{xy} and Z_{yy} terms and Z_{yx} for Z_{xx} and Z_{yx}(**N3**). These alternative normalization types affect only the contribution from the diagonal impedance terms. In addition to these cumulative RMS values, the misfits were also examined as a function of frequency.

The data considered for this study are the impedance responses from sites aqi01, aqi03, aqi04, aqi05, aqi06, aqi08, and aqi09. Most of the responses represent data files merged from different acquisition dates with different sites serving as the local and remote H-field channels. The designated remote sites for the MT responses were aqi02 and aqi15. For AMT processing, sites aqi04, aqi05, and aqi08 were most often used as remote sites. As described above, much of the 2013 data were processed without a remote reference, and using aqi02 as a local magnetic field. These data were not combined with the remote referenced responses, and so the comparison of these two types of 2013 responses (locally-processed and remote-processed) with the 2014 dataset was done separately. Unfortunately, the remote referenced data from the 2013 dataset consists entirely of AMT responses so the impedance comparison is limited to periods of <3 s. This period range may or may not cover the response of interest at Aquistore (the storage complex for CO_2) but does provide a measure of MT response repeatability nonetheless.

AQI01

For aqi01, there is no remote referenced 2013 response, so the misfit calculations will include only the 2013 locally processed data and the 2014 remotely processed data (Table 4). The majority of the MT responses are based on aqi01 and aqi10 H-field data, while the nearby aqi05 site and the much more distant aqi12 are used as local magnetic channels in AMT responses. The combined 2014 response used four different remote reference sites. It is immediately apparent that the data editing for of the 2014 response has restricted the amount of common frequency data between the two surveys (Figure 11). For this site, there are two bands within which the data can be compared: 0.01 to 1 s and 10 to ~2000 s. It is also clear that the off-diagonal terms, Z_{xy} and Z_{yx}, exhibit a high level of agreement between the two responses. In contrast, for the diagonal terms, the 2014 data are significantly noisier in the 0.01 to 1 s band. Noise in the diagonal terms is to be expected for dominantly layered earth electrical structure incapable of generating signals in those components.

Table 4 Local/Remote import magnetic channels for aqi01 data

		21-Aug	22-Aug	23-Aug	
2013	MT	aqi01/	aqi01/		
	AMT			aqi05/	
		7-Nov	8-Nov	11-Nov	12-Nov
2014	MT	aqi01 /aqi02	aqi01/aqi02	aqi10/aqi15	aqi10/aqi15
	AMT	aqi05/aqi04	aqi05/aqi04	aqi12/aqi11	aqi12/aqi11

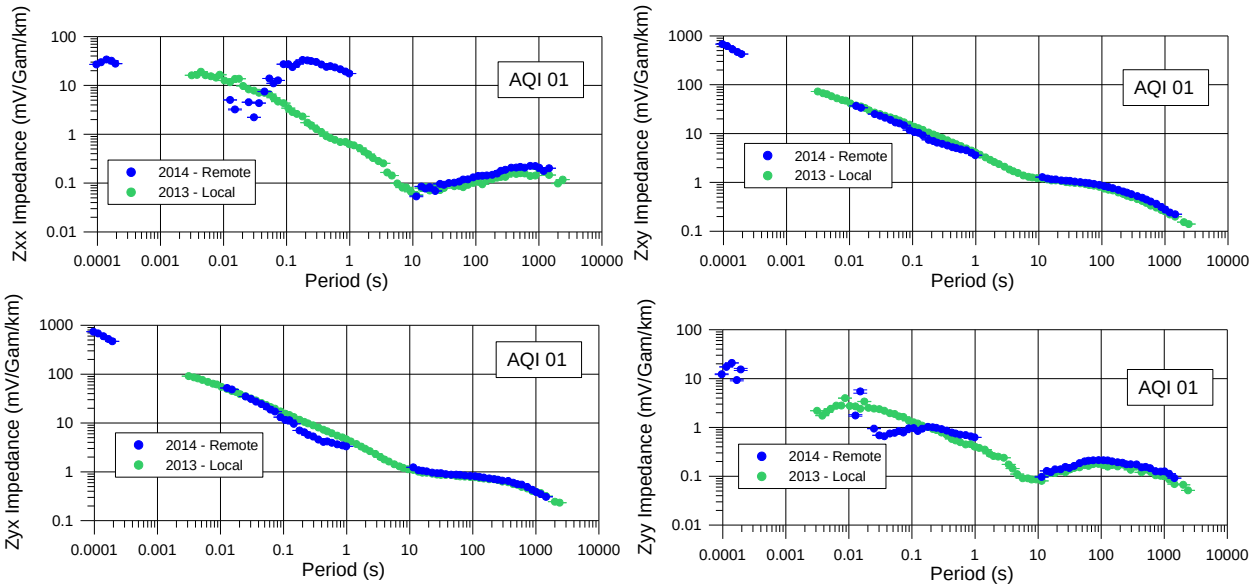

Figure 11 Comparison of impedance magnitude data at aqi01 from 2013 and 2014 surveys. Clockwise from top-left: Zxx, Zxy, Zyx, Zyy.

Using the **N1** normalization, the cumulative RMS is 1.2601 (Figure 12). The contributions of the off-diagonal terms are negligible compared to the short period Z_{xx} and Z_{yy} misfits. The results using **N2** and **N3** show an improvement but the high values of Z_{xx} in 2014 continue to dominate results. The **N2** misfit, which assumes electric field noise, generates the smallest misfit.

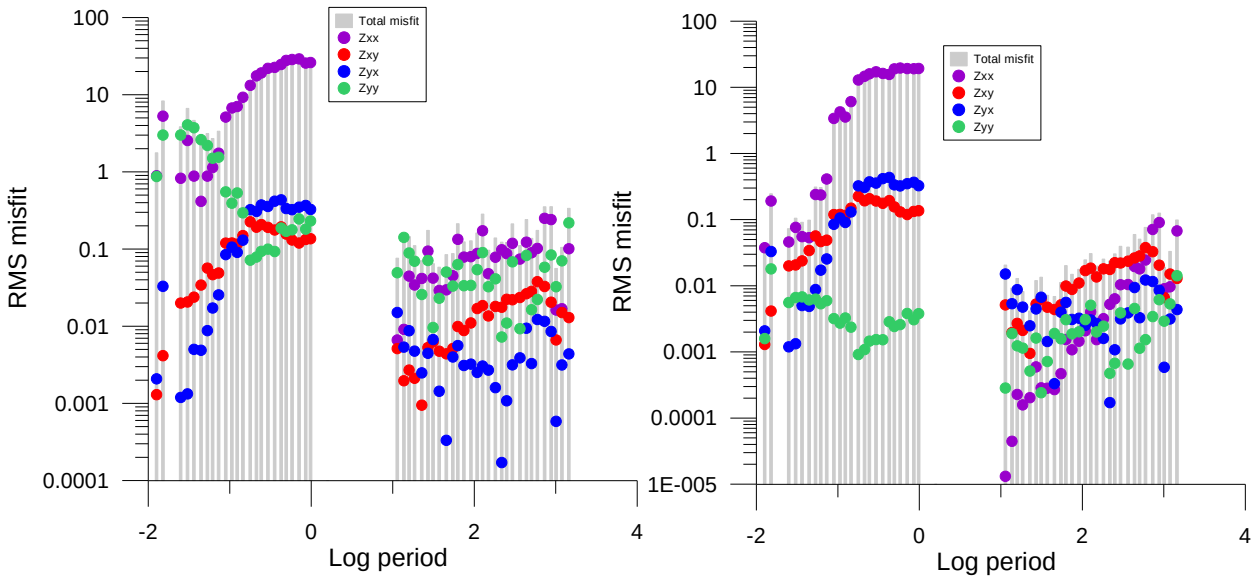

Figure 12 RMS N1 (left) and N2 (right) misfit for all four impedance terms at aqi01. The sum of the four misfit terms is shown by the grey bars. RMS_{N1}: 0.8910, RMS_{N2}: 0.7132.

The results for aqi01 show good repeatability (<0.03 or 3%) at periods less than about 0.03 s and longer than 1 s. However, there is a one to two order of magnitude increase in the Z_{xy} and Z_{yx} misfit as the period increases from about 0.1 s to 1 s. This increase occurs in the period band adjacent to the band of responses removed because of their obvious noise effects. The observations suggest that the effect of the noise extend to shorter periods where their effect is less obvious in the impedance data. As a result the repeatability misfit determination will be biased upwards. However, the plots produced in the misfit calculation provide a useful way of characterizing significant noise effects in the impedance.

AQI03

There were no magnetic field sensors made available at the aqi03 site, and so all magnetic field data in these responses have been imported from elsewhere (Table 5). After editing, there is very little data overlap at site aqi03 between the two sets of remote referenced data (Figure 13).

Table 5 Local/Remote import magnetic channels for aqi03 data

		22-Aug	23-Aug	26-Aug
2013	MT	aqi01/		aqi02/
	AMT		aqi05/	aqi05/aqi08
		7-Nov		
2014	MT	aqi01/aqi02		
	AMT	aqi05/aqi04		

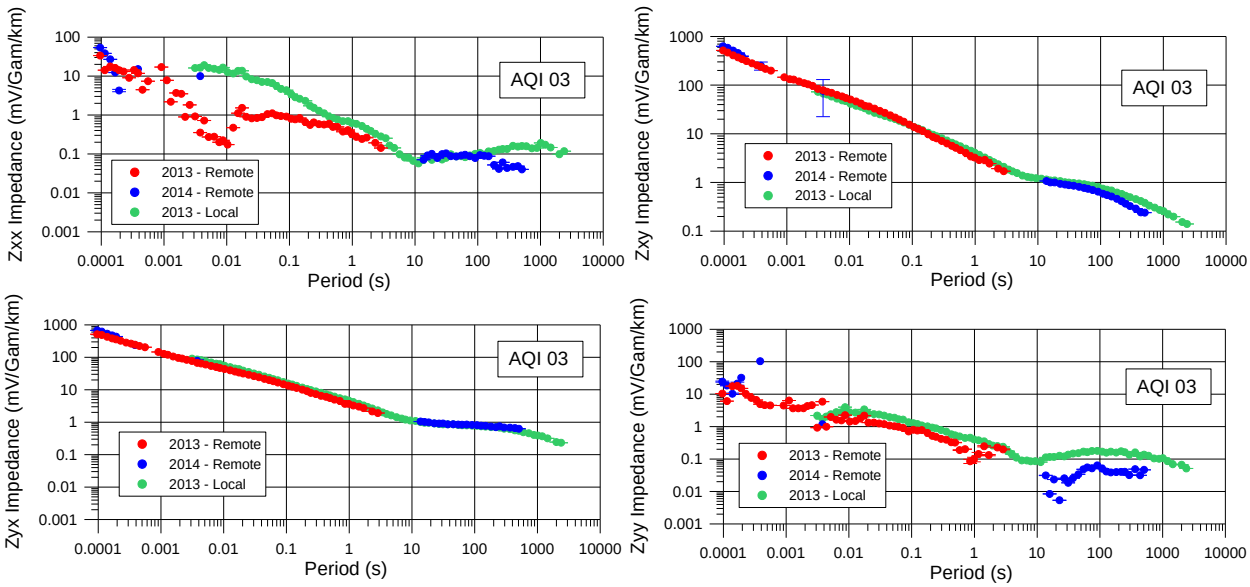

Figure 13 Comparison of impedance magnitude data at aqi03 from 2013 and 2014 surveys. Clockwise from top-left: Zxx, Zxy, Zyx, Zyy.

The misfit calculations for 2013 and 2014 remote-referenced responses show that the diagonal terms once again have much larger misfits (Figure 14). The results suggest that a reasonable misfit could have been obtained from the off-diagonal terms if such extensive editing had not been required; the long period data from 2014 appears to be following the trend of the shorter period 2013 impedances.

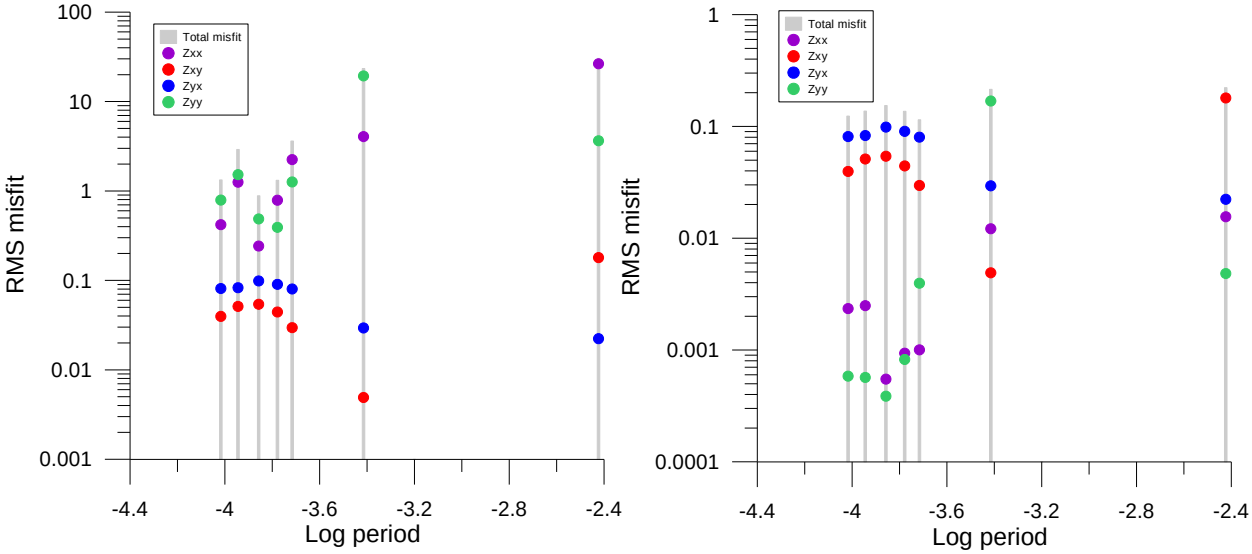

Figure 14 RMS N1 (left) and N2 (right) misfit for all four impedance terms at aqi03 – 2013 remote/2014 remote. The sum of the four misfit terms is shown by the grey bars. RMS_{N1}: 1.0672, RMS_{N2}: 0.1404.

Replacing the remote-referenced 2013 responses with locally processed data allows for comparison of the datasets at longer periods (Figure 15). In this period range, the highest misfits are for the Z_{xx} and Z_{yy} terms. The **N2** and **N3** calculations reduce the misfit significantly. There does not appear to be a much frequency variation of the misfit for impedance term.

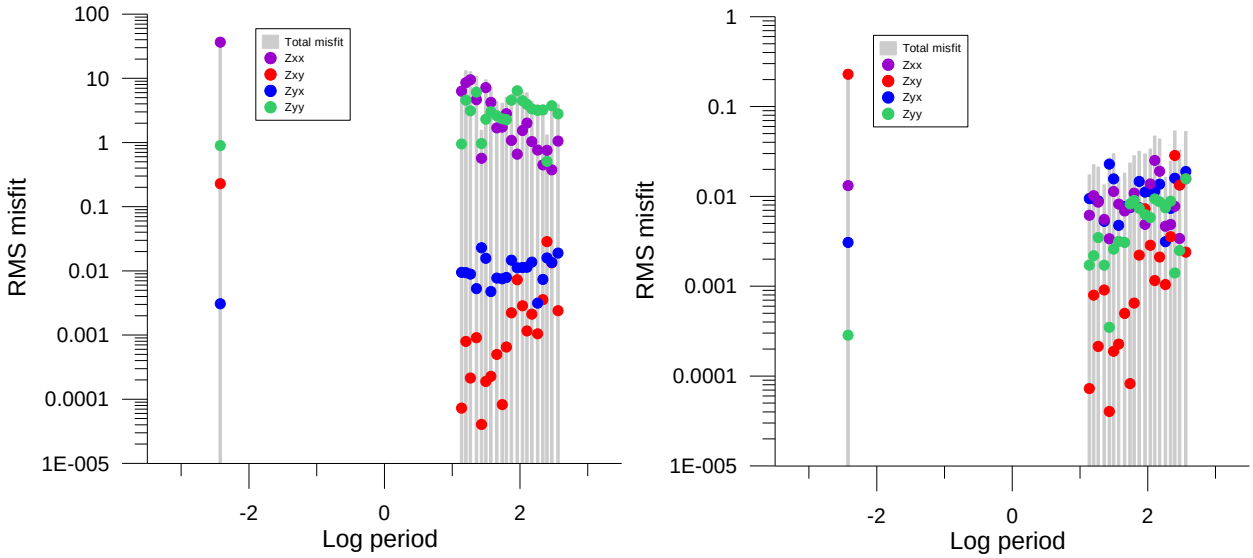

Figure 15 RMS N1 (left) and N2 (right) misfit for all four impedance terms at aqi03– 2013 local/2014 remote. The sum of the four misfit terms is shown by the grey bars. RMS_{N1}: 0.9738, RMS_{N2}: 0.0702.

AQI04

At aqi04, the local H-field was never imported from another site for AMT processing, while the MT-processed responses were highly dependent on aqi01 (Table 6).

Table 6 Local/Remote import magnetic channels for aqi04 data

		22-Aug	26-Aug
2013	MT	aqi01/	aqi02/
	AMT	aqi04/aqi05	aqi04 /aqi08
		7-Nov	8-Nov
2014	MT	aqi01/aqi02	aqi01/aqi02
	AMT	aqi04 /aqi05	aqi04 /aqi05

The repeatability of the Z_{xy} and Z_{yx} data appears high, but the diagonal terms are very noisy for both surveys (Figure 16). The 2014 remote Z_{yy} data in particular appears to be biased upwards by about a decade from the 2013 magnitudes. This effect completely dominates the **N1** RMS for comparison of the remote data. The **N2** and **N3** calculations provide improved misfit estimates with RMS values of 0.0846 and 0.0851, respectively (Figure 17).

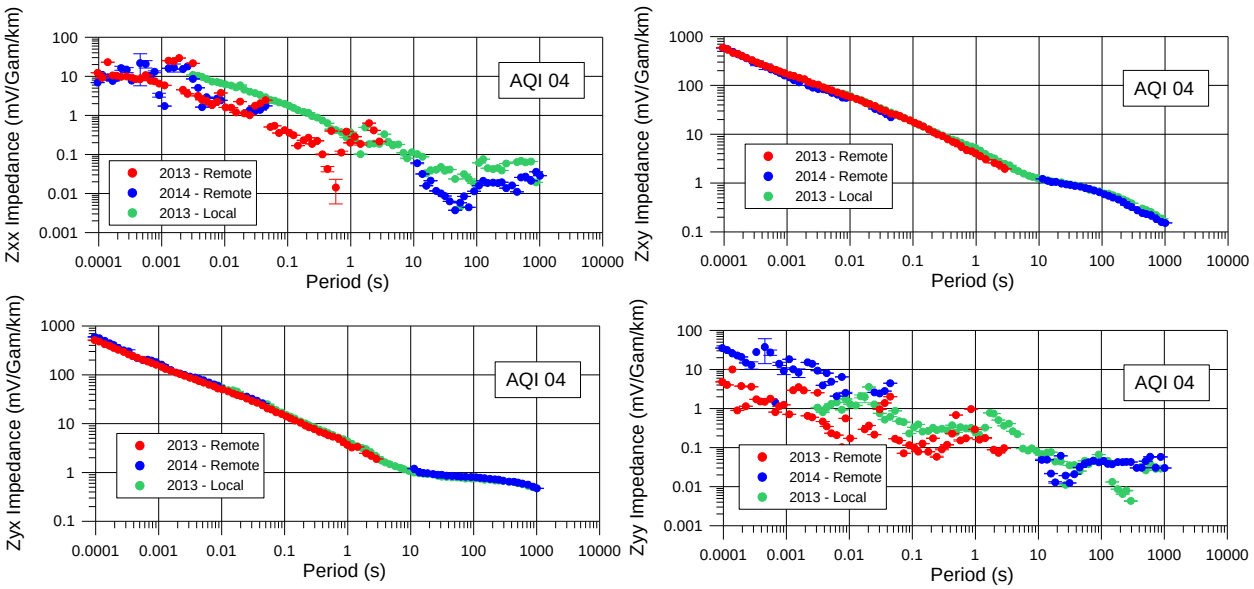

Figure 16 Comparison of impedance magnitude data at aqi04 from 2013 and 2014 surveys. Clockwise from top-left: Zxx, Zxy, Zyx, Zyy.

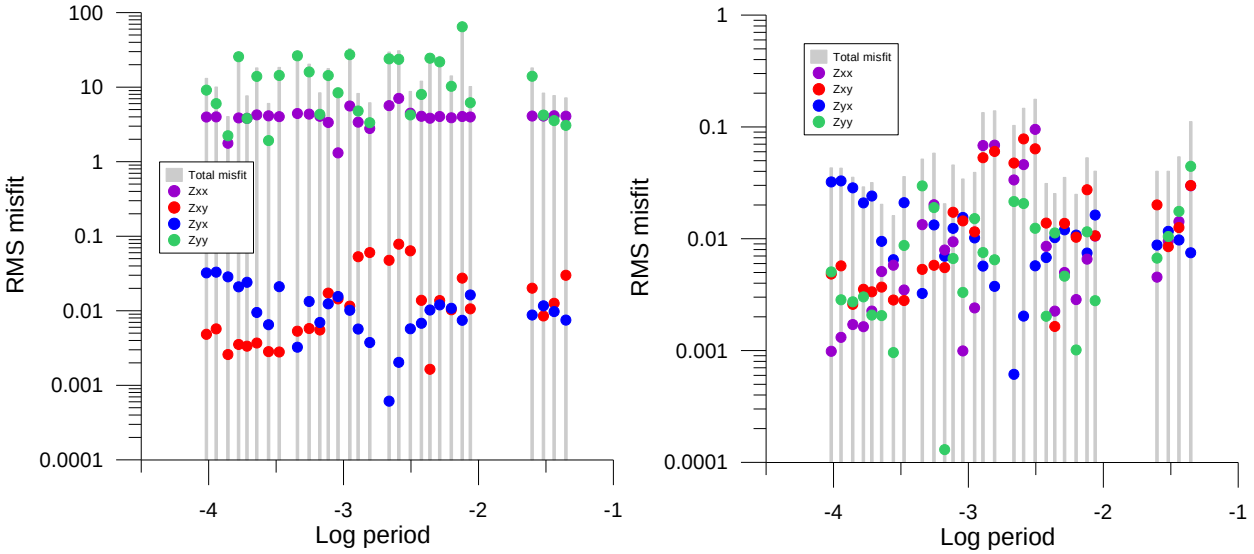

Figure 17 RMS N1 (left) and N2 (right) misfit for all four impedance terms at aqi04 – 2013 remote/2014 remote. The sum of the four misfit terms is shown by the grey bars. RMS_{N1}: 1.4839 RMS_{N2}: 0.0846.

Using the local 2013 responses, we can once again compare the datasets at much longer periods (Figure 18). The noisy diagonal terms lead to high misfits for the **N1** calculation. The misfit improvement in **N2** and **N3** alternate calculations does not show a consistent pattern of the misfit among impedance terms. Over much of frequency range the misfit is less than 0.05 (or 5%). However, the results again show an increase in misfit adjacent to the noise band.

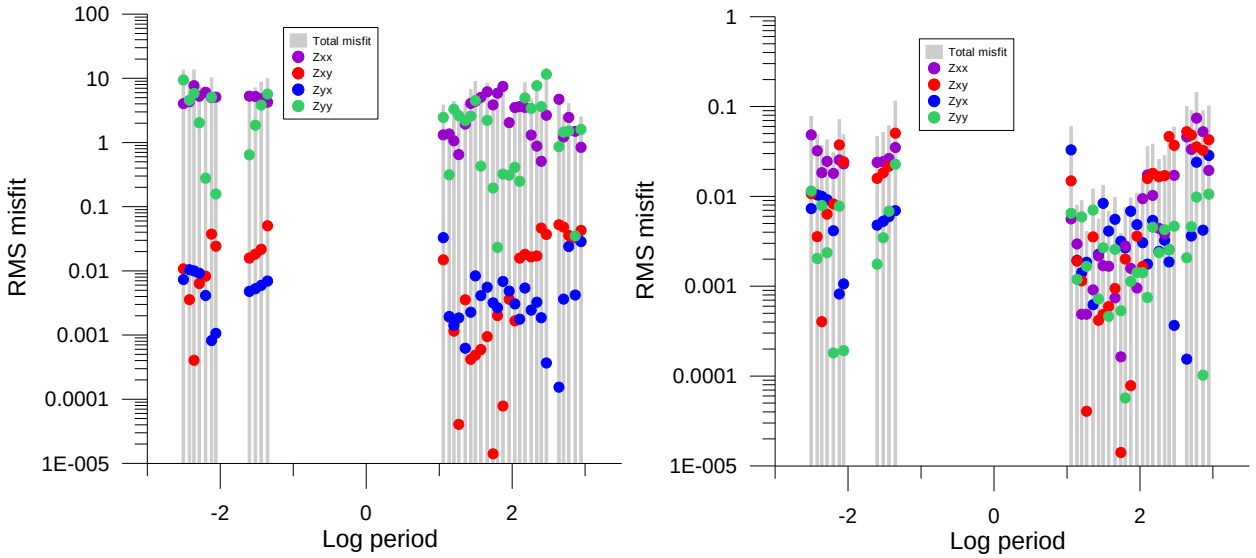

Figure 18 RMS N1 (left) and N2 (right) misfit for all four impedance terms at AQI04 – 2013 local/2014 remote. The sum of the four misfit terms is shown by the grey bars. RMS_{N1}: 0.8900, RMS_{N2}: 0.0738.

AQI05

As for aqi01, the high aqi05 misfits are related mainly to the 2014 Z_{xx} response between 0.01 and 1 s (Figure 19). There is no imported local H-field data in the 2014 AMT band (Table 7). For aqi01, some aqi05 magnetic field data were imported in the 2014 data processing.

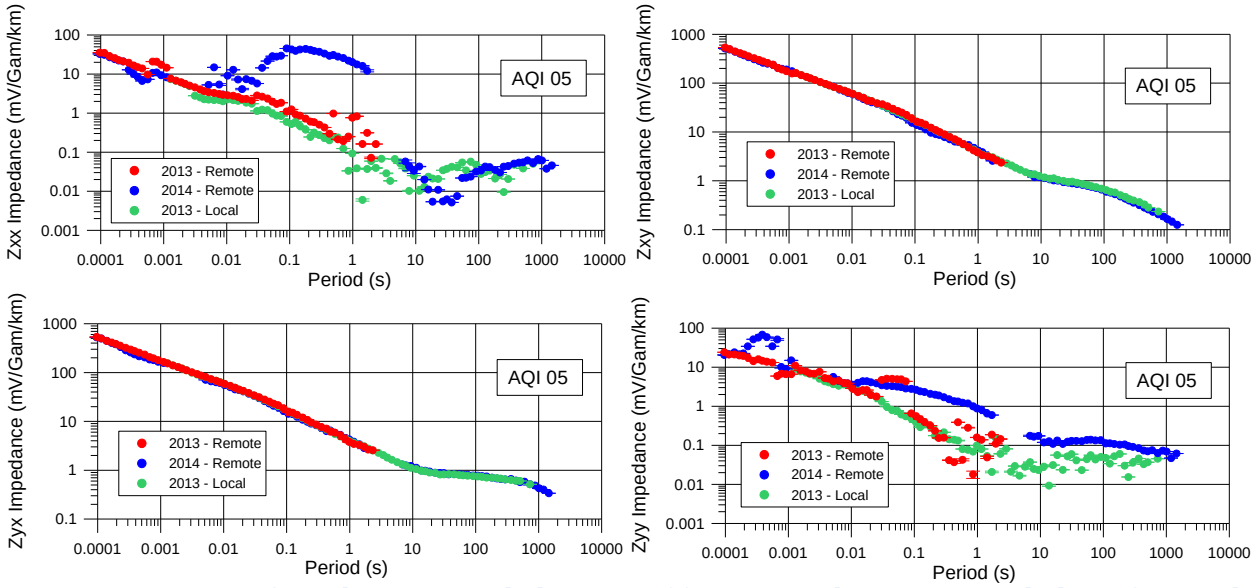

Figure 19 Comparison of impedance magnitude data at aqi05 from 2013 and 2014 surveys. Clockwise from top-left: Zxx, Zxy, Zyx, Zyy.

The high misfit in the 0.01 to 1 s band can be seen in the calculations for both the local and remote 2013 data (Figure 20 and Figure 21). The Z_{yy} misfit is lowered considerably when using the **N2** or **N3** types of normalization, but the Z_{xx} misfit remains high. There is a significant increase in the misfit of off-diagonal impedance terms adjacent to the noise band and at long periods.

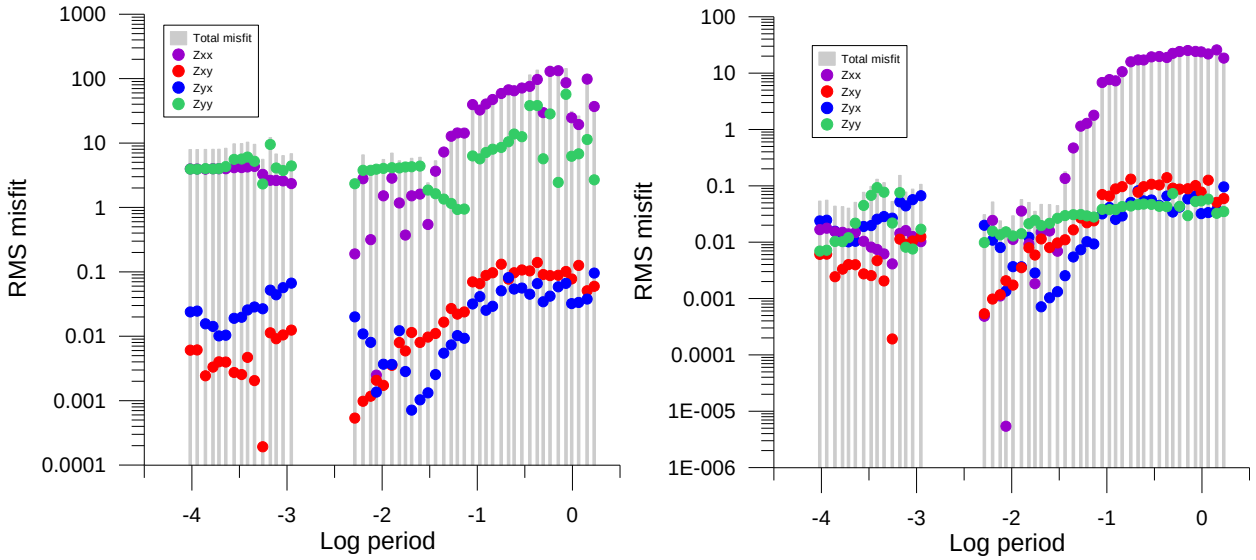

Figure 20 RMS N1 (left) and N2 (right) misfit for all four impedance terms at aqi05 – 2013 remote/2014 remote. The sum of the four misfit terms is shown by the grey bars. RMS_{N1}: 2.0590, RMS_{N2}: 0.9268.

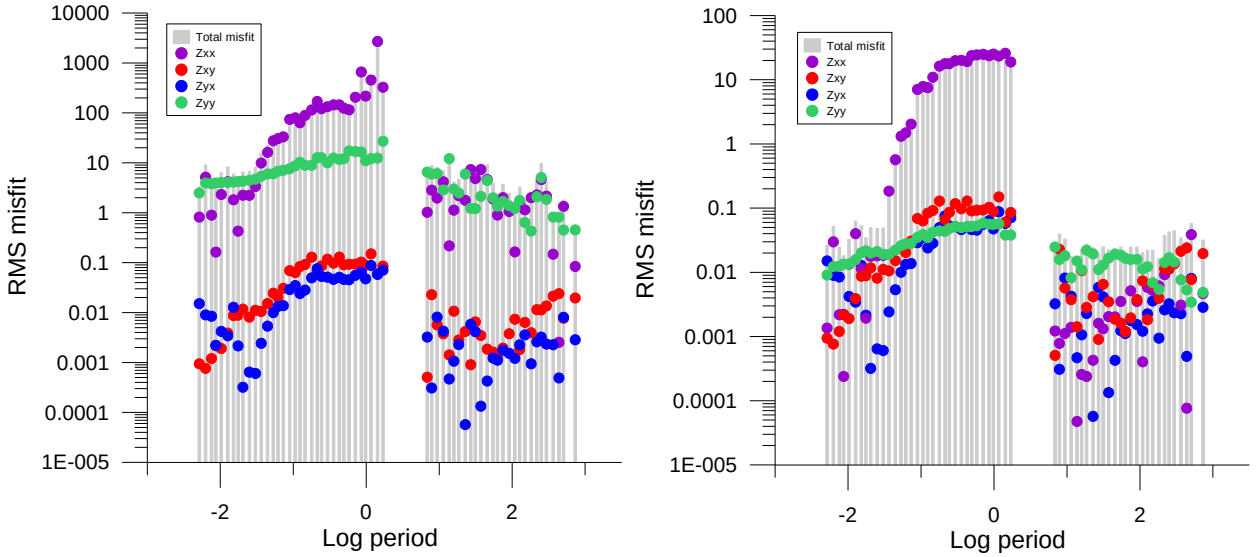

Figure 21 RMS N1 (left) and N2 (right) misfit for all four impedance terms at aqi05 – 2013 local/2014 remote. The sum of the four misfit terms is shown by the grey bars. RMS_{N1}: 3.6561, RMS_{N2}: 0.8409.

Table 7 Local/Remote import magnetic channels for aqi05 data

		22-Aug	23-Aug	24-Aug	25-Aug	26-Aug
2013	MT	aqi01/		aqi02/	aqi02/	
	AMT	aqi05 /aqi04	aqi05/	aqi05 /aqi08	aqi05 /aqi08	aqi05 /aqi04
		7-Nov	8-Nov	9-Nov		
2014	MT	aqi01/aqi02	aqi01/aqi02	aqi09/aqi15		
	AMT	aqi05 /aqi04	aqi05 /aqi04	aqi05 /aqi08		

AQI06

The local H-fields for aqi06 were imported from numerous different sites (Table 5). As with aqi03, for aqi06 there is very little overlapping data between remote referenced 2013 and 2014 responses (Figure 22). The misfits are generally low (Figure 23 and Figure 24), however it is clear that the **N2** and **N3** type normalizations once again remove the effect of noisier Z_{xx} and Z_{yy} data to generate smaller, more evenly distributed misfits.

Table 8 Local/Remote import magnetic channels for aqi06 data

		22-Aug	23-Aug	24-Aug
2013	MT	aqi01/		aqi02/
	AMT	aqi05/aqi04	aqi05/	aqi08/aqi05
		9-Nov	10-Nov	
2014	MT	aqi09/aqi15	aqi10/aqi15	
	AMT	aqi05/aqi08	aqi08/aqi12	

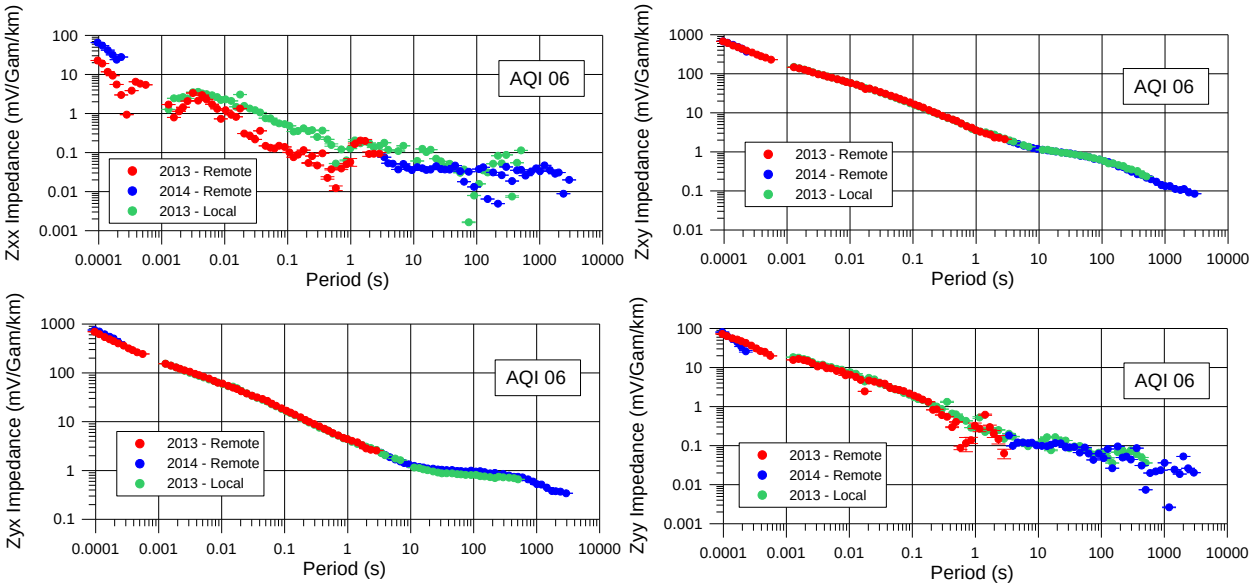

Figure 22 Comparison of impedance magnitude data at aqi06 from 2013 and 2014 surveys. Clockwise from top-left: Zxx, Zxy, Zyx, Zyy.

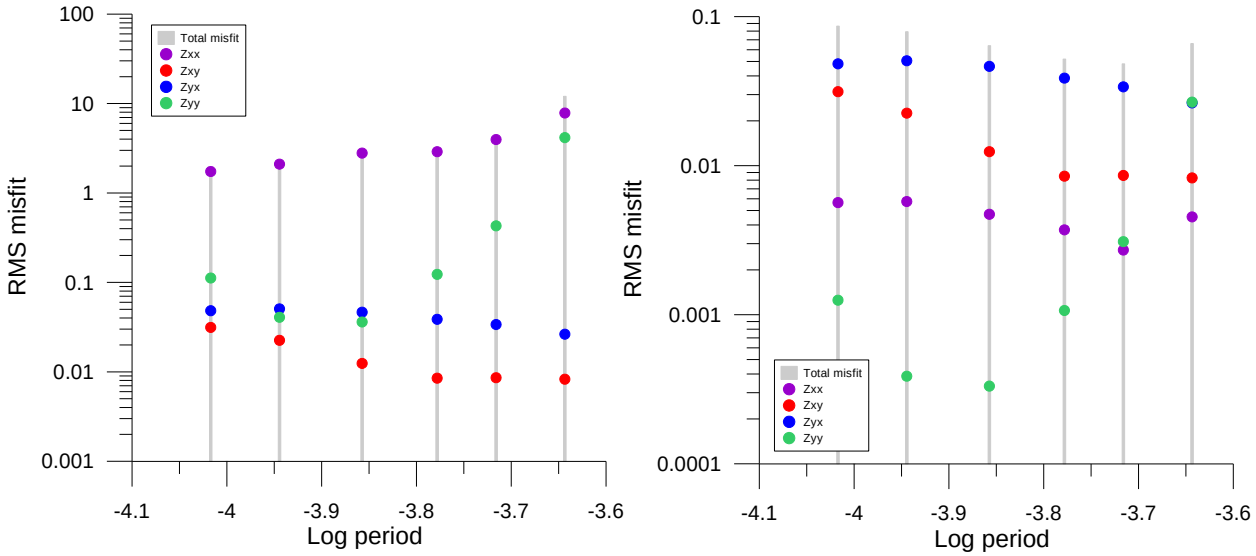

Figure 23 RMS N1 (left) and N2 (right) misfit for all four impedance terms at aqi06 – 2013 remote/2014 remote. The sum of the four misfit terms is shown by the grey bars. RMS_{N1}: 0.7440, RMS_{N2}: 0.0908.

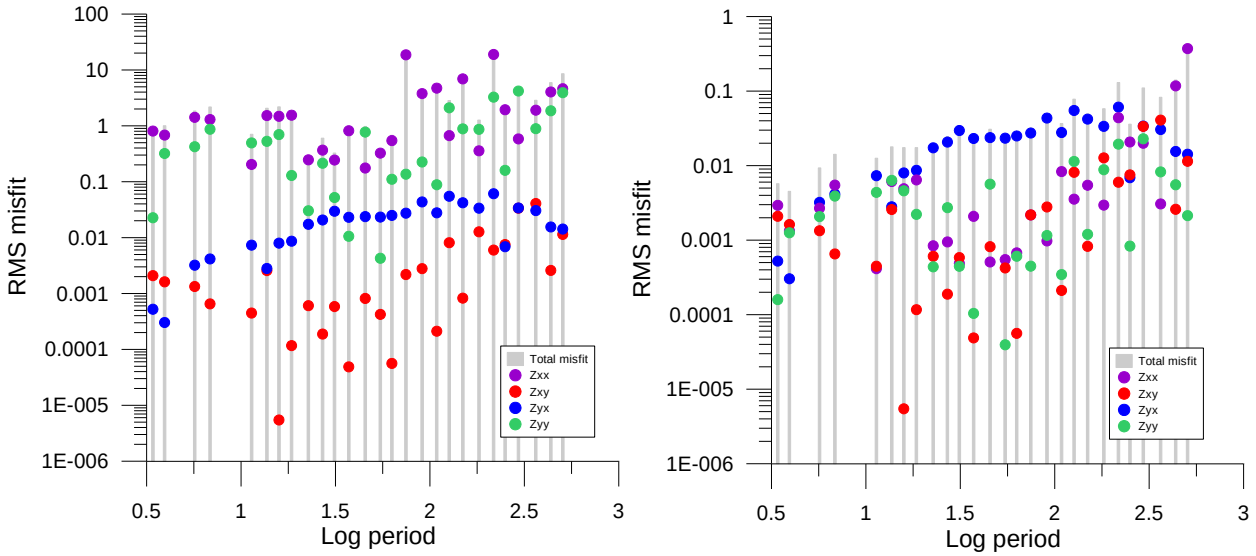

Figure 24 RMS N1 (left) and N2 (right) misfit for all four impedance terms at aqi06 – 2013 local/2014 remote. The sum of the four misfit terms is shown by the grey bars. RMS_{N1}: 0.6897, RMS_{N2}: 0.0829.

AQI08

The MT-processed data for aqi08 (Figure 25) used magnetic field data imported from various other sites: aqi02, aqi09, and aqi10 (

Table 9). For the short period range in which the 2013 remote referenced responses were compared to those from 2014, the highest misfit is attributed to the Z_{xx} term, for which the 2014 data is noisy. This is reflected in the **N1** misfit calculation. For the subsequent **N2** and **N3** calculations, the misfits are significantly lower, but generally are still highest for the Z_{xx} term. The results are similar in the longer period range (Figure 26 and Figure 27). An outlier in the distribution of the misfit corresponds to a 2014 Z_{xx} data point at 0.1 s. The results show a very clear increase in misfit adjacent to the noise band.

Table 9 Local/Remote import magnetic channels for aqi08 data

		24-Aug	25-Aug	26-Aug
2013	MT	aqi02/	aqi02/	
	AMT	aqi08 /aqi05	aqi08 /aqi05	aqi08 /aqi04
		9-Nov	10-Nov	
2014	MT	aqi09/aqi15	aqi10/aqi15	
	AMT	aqi08 /aqi05	aqi08 /aqi12	

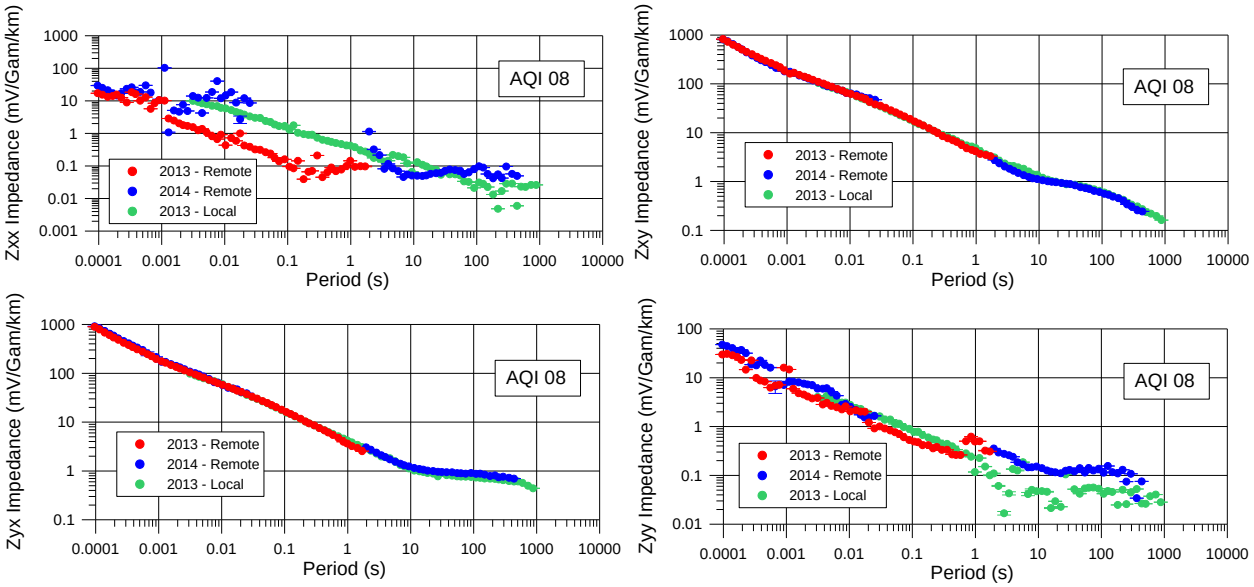

Figure 25 Comparison of impedance magnitude data at aqi08 from 2013 and 2014 surveys. Clockwise from top-left: Zxx, Zxy, Zyx, Zyy.

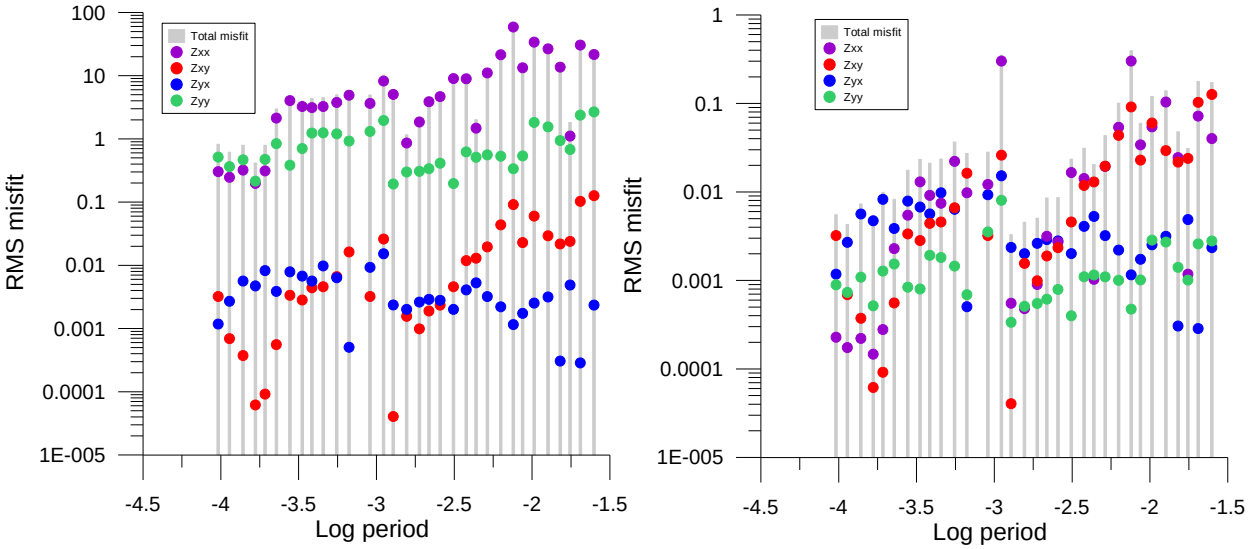

Figure 26 RMS N1 (left) and N2 (right) misfit for all four impedance terms at aqi08 – 2013 remote/2014 remote. The sum of the four misfit terms is shown by the grey bars. RMS_{N1}: 1.1406, RMS_{N2}: 0.0875.

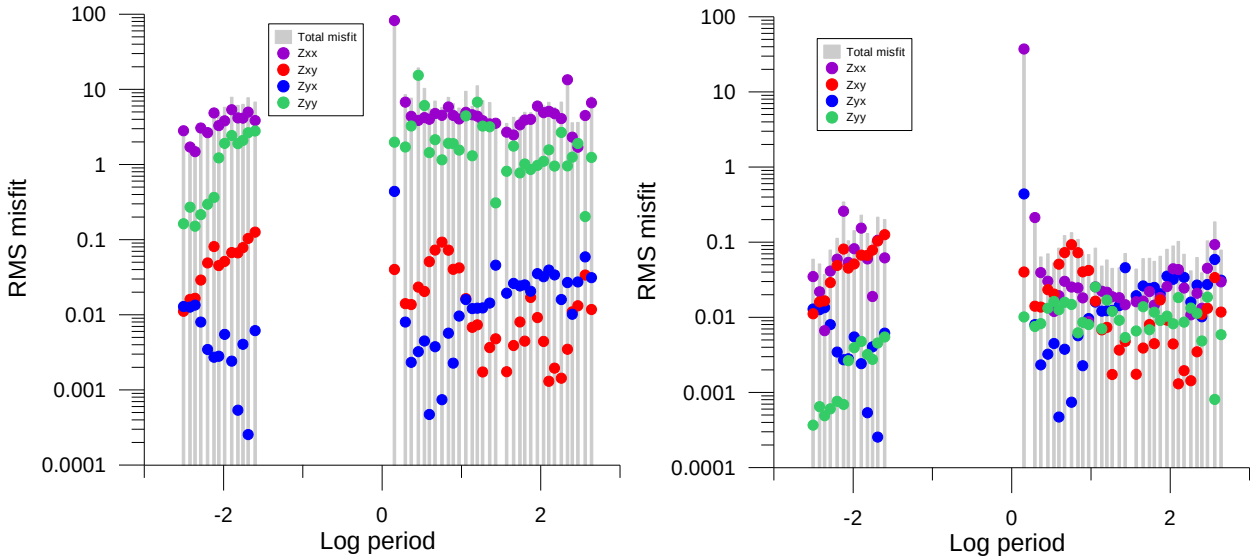

Figure 27 RMS N1 (left) and N2 (right) misfit for all four impedance terms at aqi08 – 2013 local/2014 remote. The sum of the four misfit terms is shown by the grey bars. RMS_{N1}: 1.0066, RMS_{N2}: 0.3417.

AQI09

Magnetic field data from aqi09 was only used once: as part of the MT-processed 2014 response. A variety of other H-field channels were imported for data processing (Table 10). The diagonal terms show noisy data, especially for the 2014 survey and for the Z_{yy} term (Figure 28). Calculations of the misfit for both local and remote-referenced 2013 responses produced similar results (Figure 29 and Figure 30). The misfit is lowered greatly when switching from **N1** type normalization to **N2** or **N3**, though the Z_{yy} misfit remains the highest at periods less than 1 s.

Table 10 Local/Remote import magnetic channels for aqi09 data

		24-Aug	25-Aug
2013	MT	aqi02/	aqi02/
	AMT	aqi08/aqi05	aqi08/aqi05
		9-Nov	10-Nov
2014	MT	aqi09 /aqi15	aqi10/aqi15
	AMT	aqi08/aqi05	aqi08/aqi12

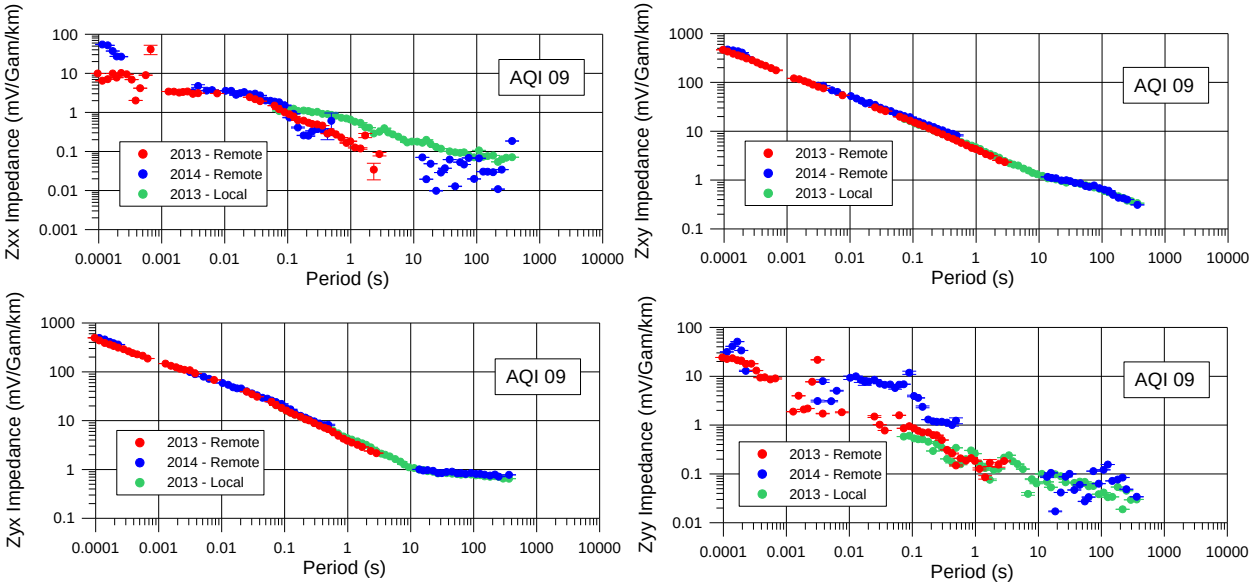

Figure 28 Comparison of impedance magnitude data at aqi09 from 2013 and 2014 surveys. Clockwise from top-left: Zxx, Zxy, Zyx, Zyy.

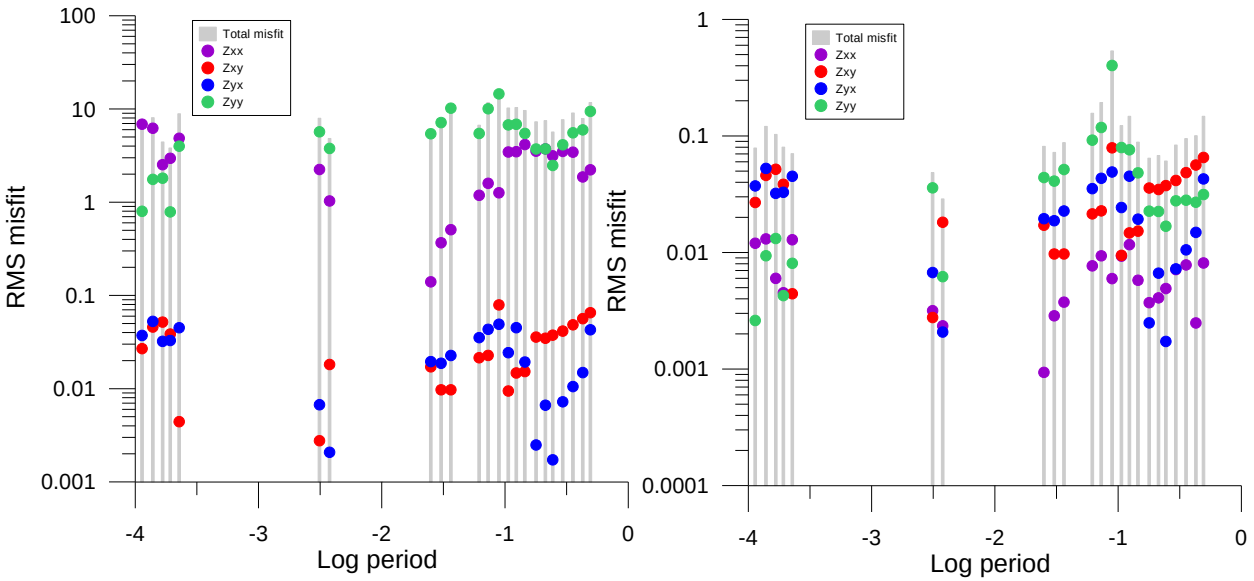

Figure 29 RMS N1 (left) and N2 (right) misfit for all four impedance terms at aqi09 – 2013 remote/2014 remote. The sum of the four misfit terms is shown by the grey bars. RMS_{N1}: 1.0188, RMS_{N2}: 0.1197.

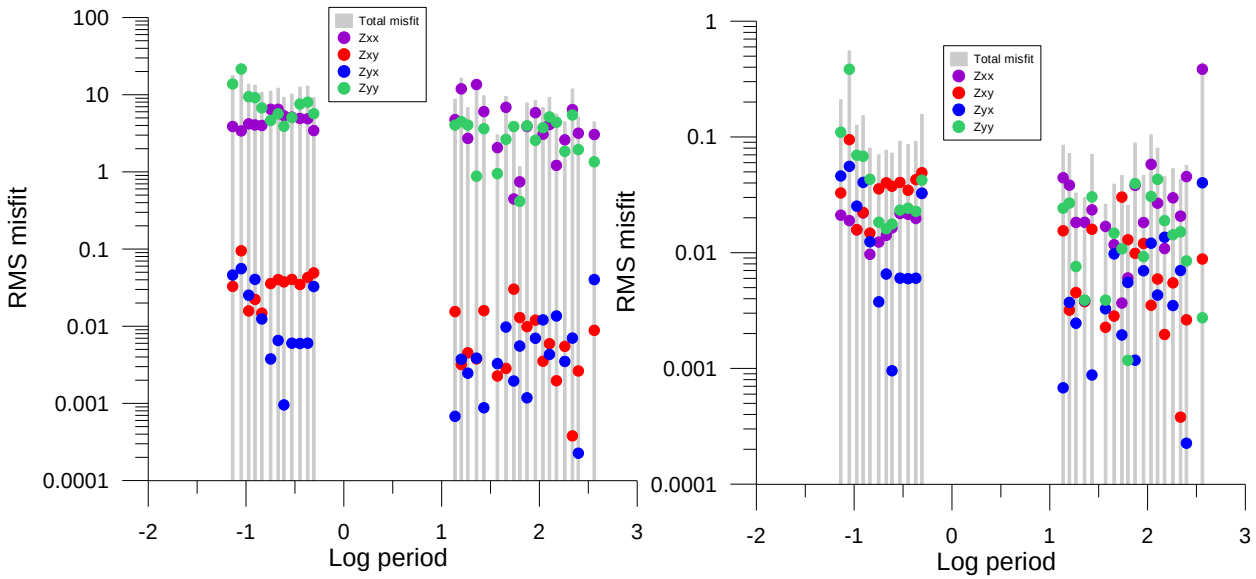

Figure 30 RMS N1 (left) and N2 (right) misfit for all four impedance terms at aqi09 – 2013 local/2014 remote. The sum of the four misfit terms is shown by the grey bars. RMS_{N1}: 1.1104, RMS_{N2}: 0.1146.

Discussion

The strongest limiting factor in the computation of misfit values between 2013 and 2014 MT data was the restricted number of common frequencies available after the editing of the responses and the lack of remote referenced long-period 2013 responses. A section of the 2014 data in the period range of 1 to 10 s has been edited out, and data over the extended range of 0.01 to 10 s at some sites. There remain substantial bias effects from the noise on much of the unedited data. This is because the editing was based primarily on the variance of the apparent resistivity and phase responses for the *XY* and *YX* terms. The increase in misfit adjacent to the noise band at a number of the sites indicates the presence of residual effects of the noise.

Visual inspection of the impedance responses indicates that outside the noise band the off-diagonal impedance terms are quite consistent from survey to survey. The impedance magnitudes are similar so static shift associated with the re-installation of electrodes between surveys does not appear to be a significant issue.

The results of the misfit calculations are summarized in Table 11 and Table 12. Overall, the misfit values are high. For every site, the misfits are highest for **N1** normalization. This result indicates the presence of large relative errors on the diagonal impedance terms. This result is expected as no signal is predicted in the diagonal terms for a layered earth. The **N2** and **N3** misfit values for aqi01, aqi05 and aqi08 are also very high (~1) and inspection of the misfit curves shows that for all three of these sites the **N2** and **N3** misfit is still dominated by the diagonal impedance terms. The misfit on the diagonal terms is larger than the magnitude of the off-diagonal impedance. The **N2** and **N3** misfit values for aqi03, aqi04, aqi06 and aqi09 are significantly lower, and typically lie between 0.07 and 0.11 indicating average misfits of 7 to 11%. The frequency dependent plots indicate that a high component of this misfit arises at very high and very low periods, and periods adjacent to the 2014 noise band.

Differences in the results between **N2** and **N3** are minimal both in terms of the cumulative RMS, and the distribution of the misfit among the separate impedance terms.

The methodology that has been established to parameterize the misfit between sets of MT data appears to be very functional. However, the parameterization of the repeatability of the MT survey data is severely impacted by the level and form of noise in the 2014 MT data. This noise required the editing of large portions of the 2014 data limiting the period range in which the 2013 and 2014 responses could be compared. In addition, it caused bias of the MT responses in bands adjacent to those in which the noise was evident during the data editing and the polarization of the noise severely biased diagonal impedance elements upwards.

Table 11 Summary of RMS calculations - 2013 local against 2014 remote

	AQI01	AQI03	AQI04	AQI05	AQI06	AQI08	AQI09
RMS-N1	0.8910	0.9738	0.8900	3.6561	0.6897	1.0066	1.1104
RMS-N2	0.7132	0.0702	0.0738	0.8409	0.0829	0.3417	0.1146
RMS-N3	0.7254	0.0730	0.0730	0.8296	0.0767	0.3631	0.1132
Data points	53	21	36	61	27	45	30

Table 12 Summary of RMS calculations - 2013 remote against 2014 remote

	AQI03	AQI04	AQI05	AQI06	AQI08	AQI09
RMS-N1	1.0672	1.4839	2.0590	0.7440	1.1406	1.0188
RMS-N2	0.1404	0.0846	0.9268	0.0908	0.0875	0.1197
RMS-N3	0.1403	0.0851	0.9108	0.0911	0.0901	0.1257
Data points	7	29	49	6	32	23

From 0.1 to 10 s, there is a consistently low signal to noise ratio and low coherences throughout both datasets. This coincides with the period range of high misfit for aqi05. The behaviour of the 2014 AQI05 Z_{xx} term in this range is repeated frequently and to a lesser degree in the datasets, but is usually not expressed in the combined, edited responses, aqi01 being the exception. It is generally seen from the unedited responses that these effects are stronger for the 2014 dataset. A possible explanation is that some additional infrastructure (e.g. pipeline) constructed near to the injection well in between surveys has become an additional source of noise. Noting this result, it will be important to retest the repeatability of the MT once the operations around the injection well have stabilized

Conclusions and Future Work

The 2013 and 2014 surface EM surveys at Aquistore have recorded MT time series that allow the calculation of the MT response at approximately ten sites for the period range from 10^{-4} to 300 s. Using conventional MT processing procedures the data from 2013 have been used to produce high quality MT responses over this period range.

The 2014 MT data set is impacted by the presence of very high levels of EM noise. This noise has its strongest effect on the MT responses in the period range 0.1 to 10 s where it produces extreme variance and some bias of the impedance terms and requires the data points in this range to be edited out of the final response at each site. The noise also produces some bias of the impedance in adjacent period bands. Comparison of alternative estimates of the impedance indicates that the noise is strongest on the electric field components but also occurs in the magnetic field data. At most sites the noise is strongly polarized resulting in extreme upward bias of the diagonal impedance terms over a broad period band.

The very significant change between the 2013 and 2014 MT data sets suggests the noise is caused by additional infrastructure (e.g. a pipeline) constructed near to the injection well in between surveys. A possible source is cathodic protection signals. If present at the same levels, the noise will have a significant impact on future MT surveys at Aquistore. It would potentially require the development of specialized recording and MT processing procedures to remove or lessen its effect.

We have used the 2013 and 2014 MT data sets for developing procedures for defining the repeatability of MT surveys at the Aquistore site. The **N1** parameter is an RMS measure based on all four impedance components. Because of limited accuracy of variance estimates obtained from the robust MT processing procedures, in the **N1** parameter the changes in the MT response between surveys is normalized with respect to the magnitude of the responses. In a near 1-D electrical resistivity environment, such as at the Aquistore site, the diagonal impedance terms are much smaller than the off-diagonal terms allowing errors in the smaller terms to dominate measures such as **N1**. In order to reduce this effect we have defined the **N2** and **N3** measures which normalize differences in the diagonal impedance terms by associated diagonal terms.

The **N1**, **N2**, and **N3** measures have been calculated as a function of frequency and for the full responses for the 2013 and 2014 surveys. The editing of large portions of the 2014 data due to the noise limited the period range in which the data sets could be compared. It was also found that at sites at which the noise was strongest (aqi01, aqi05, aqi08) its bias of the diagonal impedance components was sufficiently strong to dominate all three statistical measures. At other sites (aqi03, aqi04, aqi06 and aqi09) the bias affected the **N1** measure but the **N2** and **N3** measures provided a more realistic measure of the misfit. The results for these measures lie between 0.07 and 0.11 indicating typical misfits of 7 to 11%. Inspection of the frequency-dependent results indicates that the misfit is significantly higher at very short period, very long periods, and for some site adjacent to the noise band. In other parts of the response the misfit is typically less than 0.03 or 3%.

Overall we can conclude that we have developed an effective methodology for examining the repeatability of the MT results and that these procedures are also useful for identifying residual effects of noise in the MT data sets. Based on the 2013 and 2014 MT results, and as evidenced by the low misfit, the parts of the data the sections of the responses with high misfit can be attributed to the effects of ambient electromagnetic noise rather than difficulties in replicating the field work.

Currently, we are completing constrained 1-D inversions of the MT responses as well as a 2-D analysis of the existing regional MT data set (Jones, 1982) to provide a more regional-scale picture of the background resistivity structure.

Future work will include applying the methodology we developed to the 2015 MT dataset and processing of the 2013 and 2015 CSEM data sets to separate the controlled source signals from the passive-source data, with the overarching goal of the calculation of robust, low-noise CSEM responses. In addition to the data analysis, numerical modelling of the source fields produced by the transmitter for a range of injection simulations and theoretical multidimensional modelling of MT responses associated with CO_2 injection will be completed. Future field work will also entail collection of similar datasets during and post-injection in order to determine if a signature within the responses or images is directly attributable to injection of CO_2.

Acknowledgements

Without the capable help of GroundMetrics Inc. running the transmitter for us, the CSEM study could not have been completed. Bernard Giroux at INRS is thanked for loan of his MTUs and transmitter. Tijana Livada and Brian Bancroft assisted in the collection of the 2013 MT data and Eric Roots assisted in the collection of the 2014 data set. The local farmers are kindly thanked for providing permission to use their land. SaskPower provided us space on site to stage gear and charge batteries. Saeid Cheraghi and Maurice Lamontagne provided comments and suggestions that have enhanced this report.

References

Aquistore, 2013, Aquistore web page. http://aquistore.ca/, accessed 02 August 2013.

Archie, G., 1942, The electrical resistivity log as an aid in determining some reservoir characteristics: Transactions of the American Institute of Mechanical Engineers, 146, 54–62.

Asten, M., 1988. The downhole magnetometric resistivity (DHMMR) method. Explor. Geophys., 19, 2, 12-16.

Bachu, S. and B. Hitchon. 1996. Regional-Scale Flow of Formation Waters in the Williston Basin, AAPG Bull., V.80, No. 2, pp. 248-264.

Börner, J.H., Herdegen, V., Repke, J.-U., Spitzer, K., 2013. The impact of CO_2 on the electrical properties of water bearing porous media–laboratory experiments with respect to carbon capture and storage. *Geophysical Prospecting*, Volume 61, pages 446–460.

Börner, J.H., Herdegen, V., Repke, J.-U., Spitzer, K., 2015. The electrical conductivity of CO_2-bearing pore waters at elevated pressure and temperature: a laboratory study and its implications in CO_2 storage monitoring and leakage detection. *Geophys. J. Int.*, Volume 203, pages 1072–1084.

Bosch, D., Ledo, J., Queralt, P., Bellmunt, F., Luquot, L. and Gouze, P., 2016. Core-scale electrical resistivity tomography (ERT) monitoring of CO_2–brine mixture in Fontainebleau sandstone. *Journal of Applied Geophysics*,Volume 130, pages 23-36.

Bishop, J., Lewis, R. & Stolz, N., 2000. Horses for (conductive) courses: DHEM and DHMMR. Explor. Geophys., 31, 192-199.

Binda, P.L. and Simpson, E.L. (1989): Petrography of sulphide-coated grains from the Ordovician Winnipeg Formation, Saskatchewan, Canada; *European Journal of Mineralogy*, Volume 1, pages 439-453.

Dixon, J. (2008): Stratigraphy and facies of Cambrian to Lower Ordovician strata in Saskatchewan; *Bulletin of Canadian Petroleum Geology*, Volume 56, pages 93-117.

Edwards, R.N., & Nabighian, N.M. (1991): The magnetometric resistivity method. Chapter 2, in *Electromagnetic Methods in Applied Geophysics, Volume 2, Applications*, ed. M.N. Nabighian, Society of Exploration Geophysicists, Tulsa, p. 47- 104.

Ferguson, A.G., Betcher, R.N., and Grasby, S.E. (2007): Hydrogeology of the Winnipeg Formation in Manitoba, Canada; *Hydrogeology Journal*, Volume 15, pages 573-587.

Fleury, M. and Deschamps, H., 2008, Electrical Conductivity and Viscosity of Aqueous NaCl Solutions with Dissolved CO_2, J. Chem. Eng. Data, 2008, 53 (11), pp 2505–2509, DOI: 10.1021/je800262

Fowler, C.M.R. and Nisbet, E.G, 1984, The subsidence of the Williston Basin; *Canadian Journal of Earth Sciences*, Volume 22, pages 408-415.

Gamble, TD, WM Goubeau, and J. Clarke (1979), Magnetotellurics with a remote reference, Geophysics, 44, 53–68, doi:10.1190/1.1440923

Gasperikova, E., and G. M. Hoversten, 2006, A feasibility study of nonseismic geophysical methods for monitoring geologic CO_2 sequestration: The Leading Edge, 25, 1282–1288, doi: 10.1190/1.2360621.

Gibbins, J. and Chalmers, H., 2008, Carbon Capture and Storage; *Energy Policy*, Volume 36, pages 4317-4322.

Gowan, E.J., Ferguson, I.J., Jones, A.G., and Craven, J.A., 2009, Geoelectric structure of the northeastern Williston basin and underlying Precambrian lithosphere; *Canadian Journal of Earth Sciences*, Volume 46, pages 441-464.

Hibbs, A., 2013, Test of a new BSEM configuration at Aquistore, and its application to mapping injected CO_2, June 26, 2013. BP project Task 1 report, 7 pp.

Huang, X., Bandilla, K.W., Celia, M. A., and Bachu, S., 2014, Basin-scale modeling of CO_2 storage using models of varying complexity, *International Journal of Greenhouse Gas Control*, 20, 73-86.

Johansen, S.E., Amundsen, H.E.F., Røsten, T., Ellingsrud, S., Eidesmo, T., and Bhuyian, A.H., 2005, Subsurface hydrocarbons detected by electromagnetic sounding: first break, 23, 31-36.

Jones, A.G., 1988. Static shift of magnetotelluric data and its removal in a sedimentary basin environment; *Geophysics*, Volume 53, pages 967-978.

Jones, A.G., 1993, The COPROD2 dataset: Tectonic setting, recorded MT data, and comparison of models; *Journal of Geomagnetism and Geoelectricity*, Volume 45, pages 933-955.

Jones, A.G. and Craven, J.A., 1990. The North American Central Plains conductivity anomaly and its correlation with gravity, magnetic, seismic, and heat flow data in Saskatchewan, Canada; *Physics of the Earth and Planetary Interiors*, Volume60, pages 169-194.

Jones, A.G., Ledo, J., and Ferguson, I.J. 2005. Electromagnetic images of the Trans-Hudson orogen: the North American Central Plains anomaly revealed; *Canadian Journal of Earth Sciences*, Volume 42, pages 457-478.

Jones, A.G., 2013, IRECCSEM: Evaluating Ireland's potential for onshore carbon sequestration and storage using electromagnetics, http://www.ireccsem.ie/overview.html

McLeod, J., Craven, J.A., Ferguson, I.J., Roberts, B.J., Bancroft, B. and Liveda, T., 2014, Overview of the 2013 Baseline Magnetotelluric and Controlled-Source Electromagnetic Geophysical Study

of CO2 Sequestration at the Aquistore site near Estevan, Saskatchewan; Geological Survey of Canada, Open File 7617, 23 p., doi:10.4095/293921

McLean, D.D., 1960, Deadwood and Winnipeg stratigraphy in east-central Saskatchewan; *Saskatchewan Department of Mineral Resources-Sedimentary Geology Division*, Report no. 47, 35 pages.

Ogaya, X., Ledo, J., Queralt, P., Marcuello, A., and Quinta, A., 2013, First geoelectric image of the subsurface of the Hontomin site (Spain) for CO_2 geological storage: A magnetotelluric 2D characterization; *International Journal of Greenhouse Gas Control*, Volume 13, pages 168-179.

SaskPower, 2013, SaskPower web page http://www.saskpower.com/, accessed 20 October 2013.

Simpson, F. and Bahr, K., 2005, Practical Magnetotellurics. Cambridge University Press, United Kingdom.

Smith, M. and Bend, S., 2004, Geochemical analysis and familial association of Red River and Winnipeg reservoired oils of the Williston Basin, Canada; *Organic Geochemistry*, Volume 35, pages 443-452.

Streich, R., 2016. Controlled-source electromagnetic approaches for hydrocarbon exploration and monitoring on land. *Surveys in Geophysics*, Volume *37*, pages 47-80.

Streich, R., Becken, M., and Ritter, O., 2010, Imaging of CO_2 storage sites, geothermal reservoirs, and gas shales using controlled source magnetotellurics: Modeling studies; *Chemie der Erde*, Volume 70, pages 63-75.

Vilamajó, E., Queralt, P., Ledo, J., and Marcuello, A., 2013. Feasibility of monitoring the Hontomín (Burgos, Spain) CO_2 storage site using deep EM source. *Surveys in Geophysics*, Volume 34, pages 441-461.

Vozoff, K. (1991): The magnetotelluric method. In: Nabighian, M.N. (Ed.), Electromagnetic Methods in Applied Geophysics – Volume 2 Applications. Society of Exploration Geophysicists, Tulsa, pages 641-711.

Ward, S.H & Hohmann, G.W., 1988, Electromagnetic Theory for Geophysical Applications; Chapter 4 in *Electromagnetic Methods in Applied Geophysics, Vol. I, Theory*, ed. Nabighian, M.N, Soc. Exploration Geophysicists, Tulsa, Okla, p. 131-311.

West, G.F. & Macnae, J.C., 1991, Physics of the electromagnetic induction exploration method. *Chapter 1 in* Electromagnetic Methods in Applied Geophysics, Volume 2, Part A, *edited by* Nabighian, M.N., Society of Exploration Geophysicists, Tulsa, OK, USA, pages 5-45.

Whittaker, S. and Worth, K., 2011, Aquistore: a fully integrated demonstration of the capture, transportation and geologic storage of CO_2; *Energy Procedia*, Volume 4, pages 5607-5614.

Zhdanov, M.S., Endo, M., Black, N., Spangler, L., Fairweather, S., Hibbs, A., Eiskamp, G.A., and Will, R., 2013, Electromagnetic monitoring of CO_2 sequestration in deep reservoirs; *First Break*, Volume 31, pages 71-78.

Zhu, C. and Hajnal, Z., 1993, Tectonic development of the northern Williston basin: a seismic interpretation of an east-west regional profile; *Canadian Journal of Earth Sciences*, Volume 30, pages 621-630.

Table 13 NRCan 2013 and 2014 MT Locations

	Latitude	Longitude	UTM (13) northing (m)	UTM (13) easting (m)	Comments
aqi01	49°05'30.4080"	103°04'46.2000"	5439434.8	640208.2	Immediately south of well pad. AMT/MT/CSEM.
aqi02	49°03'12.8880"	103°13'52.5720"	5434918.9	629227.7	Remote reference MT site ~12 km southwest of injection well.
aqi03	49°05'18.7080"	103°03'46.7640"	5439104.2	641422.7	Southwest of power station. AMT/MT only.
aqi04	49°06'23.6160"	103°03'09.8640"	5441127.6	642119.5	Northwest of power station. AMT/MT only.
aqi05	49°05'19.3920"	103°04'57.4320"	5439088.9	639989.1	South of well pad. AMT/MT/CSEM
aqi06	49°06'02.2320"	103°04'26.1480"	5440427.8	640589.9	West of canal. AMT/MT/CSEM.
aqi07	49°06'38.5200"	103°03'44.3880"	5441569.8	641407.9	South of Hwy 18. AMT/MT only.
aqi08	49°05'55.9320"	103°05'18.3840"	5440206.4	639535.7	West of well pad. AMT/MT only.
aqi09	49°06'41.7600"	103°05'05.6040"	5441628	639759.1	Northwest of well pad. AMT/MT only.
aqi10	49°02'35.3040"	103°07'07.8600"	5433956	637469.7	Distant inline site. AMT/MT/CSEM.
aqi11	49°03'42.9840"	103°06'31.7520"	5436064	638150.6	Distant inline site. AMT/MT/CSEM.
aqi12	49°04'54.4800"	103°05'20.9400"	5438307.7	639531.7	South of well pad. AMT/MT/CSEM
aqi13	49°06'38.9160"	103°04'04.8000"	5441571.5	640993.8	South of Hwy 18. AMT/MT only.
aqi14	49°06'36.0000"	103°03'58.1400"	5441484	641131	South of Hwy 18. AMT/MT only.
aqi15	49°15'31.8600"	102°50'07.5480"	5458486	657494	Remote reference MT site ~26 km northeast of injection well.

Table 14 2014 Survey Acquisition Details

	Run/start Date	Waypoint	Coils	Acquisition Notes
1496B06A	06-Nov-14	aqi02	Hx: MT8H7509 Hy:MT8H7319 Hz:MT8H7320	Polarity on Hy is reversed ACQ=AMT
1495B07A	07-Nov-14	aqi01	Hx:MT8H7322 Hy: MT8H7513	
1496B07A	07-Nov-14	aqi02	Hx: MT8H7509 Hy:MT8H7319 Hz:MT8H7320	Polarity on Hy is reversed
1561B07A	07-Nov-14	aqi03	Hx: none Hy: none	
1562B07A	07-Nov-14	aqi04	Hx: AMTC1172 Hy: AMTC1171	
1494B07A	07-Nov-14	aqi05	Hx: AMTC1216 Hy: AMTC1174 Hz:AMTC 1170	
1495B08A	08-Nov-14	aqi01	Hx:MT8H7322 Hy: MT8H7513	
1496B08A	08-Nov-14	aqi02	Hx: MT8H7509 Hy:MT8H7319 Hz:MT8H7320	Polarity on Hy is reversed
1561B08A	08-Nov-14	aqi03	Hx: none Hy: none	
1562B08A	08-Nov-14	aqi04	Hx: AMTC1172 Hy: AMTC1171	
1494B08A	08-Nov-14	aqi05	Hx: AMTC1216 Hy: AMTC1174 Hz:AMTC 1170	
1495B08B	08-Nov-14	aqi01	Hx:MT8H7322 Hy: MT8H7513	

1562B08B	08-Nov-14	aqi04	Hx: AMTC1172 Hy: AMTC1171	
1494B08B	08-Nov-14	aqi05	Hx: AMTC1216 Hy: AMTC1174 Hz:AMTC 1170	
1493B08B	08-Nov-14	aqi06	Hx: none Hy: none	Flash card not properly set in MTU
1561B08B	08-Nov-14	aqi14	Hx: none Hy: none	
1496B09A	09-Nov-14	aqi15	Hx: MT8H7319 Hy:MT8H7509 Hz: MT8H7320	
1493B09A	09-Nov-14	aqi06	Hx: none Hy: none	
1493B09A	09-Nov-14	aqi06	Hx: none Hy: none	
1562B09A	09-Nov-14	aqi08	Hx: AMTC1172 Hy: ATMC1171	
1495B09A	09-Nov-14	aqi09	Hx: MT8H7322 Hy: MT8H7513	
1494B09A	09-Nov-14	aqi05	Hx: AMTC1216 Hy: AMTC1174 Hz:AMTC 1170	
1561B09A	09-Nov-14	aqi14	Hx: none Hy: none	
1493B10A	10-Nov-14	aqi06	Hx: none Hy: none	
1562B10A	10-Nov-14	aqi08	Hx: AMTC1172 Hy: ATMC1171 Hz:AMTC1170	
1495B10A	10-Nov-14	aqi09	Hx: none Hy: none	
1561B10A	10-Nov-14	aqi10	Hx: MT8H7513 Hy:MT8H7322	
1494B10A	10-Nov-14	aqi12	Hx: AMTC1174 Hy: AMTC1216	
1496B10A	10-Nov-14	aqi15	Hx: MT8H7319 Hy:MT8H7509 Hz: MT8H7320	
1561B11A	11-Nov-14	aqi10	Hx: MT8H7513 Hy:MT8H7322	
1494B11A	11-Nov-14	aqi12	Hx: AMTC1174 Hy: AMTC1216	

1496B11A	11-Nov-14	aqi15	Hx: MT8H7319 Hy:MT8H7509 Hz: MT8H7320
1562B11A	11-Nov-14	aqi11	Hx: AMTC1172 Hy: AMTC1171
1493B11A	11-Nov-14	aqi03	Hx: none Hy: none Hz: AMTC1170
1495B11A	11-Nov-14	aqi01	Hx: none Hy: none

No E-lines